SCIENTIFIC REPORT

PN-III-P4-ID-PCCF-2016-0175, Contract No. PCCF18/2018

2018 – 2022

„High-k Nanoparticle Multilayer Dielectrics for Nanoelectronics and Energy Storage Applications"

„Nanostructuri particulate de tip multistrat cu constanta dielectrica ridicata cu aplicatii pentru stocarea energiei si dispozitive nanoelectronic"

Acronym: HIGHkDEVICE

Project website: http://nanomat.usv.ro/pagina-05-5-a.php

Consortium:

(Co-Coordinating Institution) Universitatea „Ștefan cel Mare" din Suceava (USV) – (Project Director: Assoc. Prof. Aurelian ROTARU)
(P1) Universitatea "Alexandru Ioan Cuza" din Iași (UAIC) – (Responsible partner: prof. Liliana MITOȘERIU)
(P2) Institutul National de Cercetare Dezvoltare pentru Fizica Materialelor (INCDFM) – (Responsible partner: dr. Ioana PINTILIE)
(P3) Institutul Național pentru Fizica Laserilor, Plasmei și Radiației (INFLPR) – (Responsible partner: dr. Aurelian MARCU)

Project Director,
Assoc. Prof. Aurelian ROTARU

Contents:

I. The project objectives 2
II. Summary of the context and overall objectives of the project 2
III. Highlights of the Scientific Results and Achievements of the HIGHkDEVICE project 2
IV. Dissemination in terms of remarkable publications 25

- Suceava 2022-

This report summarizes work performed on the HIGHkDEVICE project during the period October 2018 - November 2022

I. The project objectives:

The main goal of HIGHkDEVICE project is to rationally integrate solution-processable, monodisperse perovskite pristine and doped $BaTiO_3$ nanocrystals into high quality, close-packed dielectric films with controlled thickness and tunable dielectric properties (high dielectric breakdown field strength, low leakage current and low interface trap density), which can be integrated into solid state electronic devices, such as flexible capacitors and field effect transistors (FET).

II. Summary of the context and overall objectives of the project

The research activities of the HIGHkDEVICE project were mainly focused on the: ***(i)*** synthesis, characterization, testing and optimization of the properties of thin dielectric layers containing colloidal $BaTiO_3$ nanoparticles, as well as the development of strategies for the surface engineering of $BaTiO_3$ nanoparticles; ***(ii)*** the study of the influence of size effects and the nature of the capping agents on the ferroelectric properties of differently-sized $BaTiO_3$ cuboidal nanocrystals by using diffraction techniques (powder X-ray synchrotron X-ray and neutron diffraction); ***(iii)*** exploring the infiltration of nanoparticle layers with a low molecular weight monomer and initiating the *in-situ* polymerization process and characterizing the resulting dielectric layers; ***(iv)*** the advanced characterization of the dielectric and piezoelectric properties of individual pristine and $BaTiO_3$ cuboidal nanoparticles by using in-situ transmission electron microscopy (TEM) in tandem with scanning probe (atomic force (AFM) , Kelvin probe (KP) and piezoresponse force microscopy (PFM)) techniques; **(v)** the study of the structural, morphological, and compositional characterization of $BaTiO_3$ nanopowders and the measurement of their dielectric and ferroelectric properties; **(vi)** the use of $BaTiO_3$ colloidal nanocrystals for the fabrication of ferroelectric inks and the design of nanoparticle-based dielectric and ferroelectric films with controlled thicknesses; **(vii)** fabrication of pellets using nanoparticle-based powders and the densification of these pellets by using a spark plasma sintering method to improve their porosity and enhance their dielectric response; **(viii)** perform a comprehensive dielectric characterization of the nanopowders by using dielectric spectroscopy and piezoresponse force microscopy; **(ix)** the use of $BaTiO_3$ colloidal nanoparticles as dielectrc fillers for the rational design of polymer-ceramic nanocomposite films and membranes and their integration into capacitor devices, followed by the characterization and optimization of the performance of these capacitors; integration of the dielectric nanopowders into spinel-perovskite magnetoelectric nanocomposites with different architectural complexity (3-3 and 2-2) and the characterization and optimization of the magnetoelectric effect; **(x)** integrate the $BaTiO_3$ nanocrystal-based dielectric films into functional field effect transistors fabricated on both rigid and flexible substrates, their characterization, testing and optimization; and **(xi)** design of electrical inverters based on the obtained field effect transistors and the determination of their *d.c*. conversion characteristics.

III. Highlights of the Scientific Results and Achievements of the HIGHkDEVICE project

The results of the HIGHkDEVICE project will be divided in 9 mains achievements which follow the proposed working plan. Due to the page limitation of this report, only the most relevant results have been highlighted bellow, a more detailed description of these achievements was given in the annual and bi-annual project reports.

III. 1. Elaboration of Strategies for the Functionalization of $BaTiO_3$ Nanoparticles and their Assembly on Flat Surfaces as Dense and Highly Ordered Layered Structures.

The research performed exploited the unique solution-based batch-synthetic route developed by our group for the preparation of aggregate-free monodisperse ferroelectric $ATiO_3$ (A=Ba, Sr) nanocubes with precisely controlled sizes and shapes. Additionally, this project leveraged our ability to engineer the surface

composition of colloidal nanocrystals via ligand exchange processes, which enabled us to fabricate highly stable solutions by suspending the nanocrystals in both polar and non-polar solvents. The as-prepared colloidal nanocrystals have been individually passivated with oleic acid molecules, thereby preventing their aggregation and rendering them dispersible in non-polar solvents, a key requirement in the fabrication of the dielectric inks. Thus, several series of dielectric nanoparticles with controlled sizes and morphologies (cubic, spheres) have been synthesized, their dielectric properties were tuned, the nanocrystals being integrated into electronic devices fabricated on both rigid and flexible substrates. *One of the most important outcomes of the research performed to this stage is that $BaTiO_3$ nanocrystals synthesized by the solvothermal method proposed by our group present an acentric structure, as indicated by the results obtained by the USV, UAIC and NIMP teams in the consortium by using different laboratory techniques. These techniques included conventional X-Ray diffraction, Raman spectroscopy, piezoresponse force microscopy and measurement of the ferroelectric properties) and our results were confirmed by temperature-dependent neutron diffraction techniques, performed through a collaboration with the Oak Ridge National Laboratory (USA).* Interestingly, the real crystal structure of the nanocrystals appears to be orthorhombic, and not presumably tetragonal, structure which is also ferroelectric being associated with the off-center shift of the Ti^{4+} within the TiO_6 octahedra, which could lead to high values of the dielectric constant and a robust ferroelectric behavior at room temperature. In conclusion, all the objectives planned to be achieved at this stage of research have been 100% achieved, the results obtained being very promising in carrying out the subsequent activities provided in the project. A constant effort during the two years of the project was to fabricate $BaTiO_3$ colloidal nanocrystals with different sizes and surface composition (Thrust 1) by using a highly reliable, low cost solvothermal technique and to optimize the reaction conditions in order to improve the size distribution of the resulting nanocrystals. As such, the first step was focused on the optimization of the synthesis conditions of $BaTiO_3$ nanoparticles with cuboidal shape. To this end, a systematic study of the role played by different factors (solvent polarity, reaction time, reaction temperature, molar ratio between precursors, solvent and passivation agent, etc.) on the morphology of nanoparticles was performed.

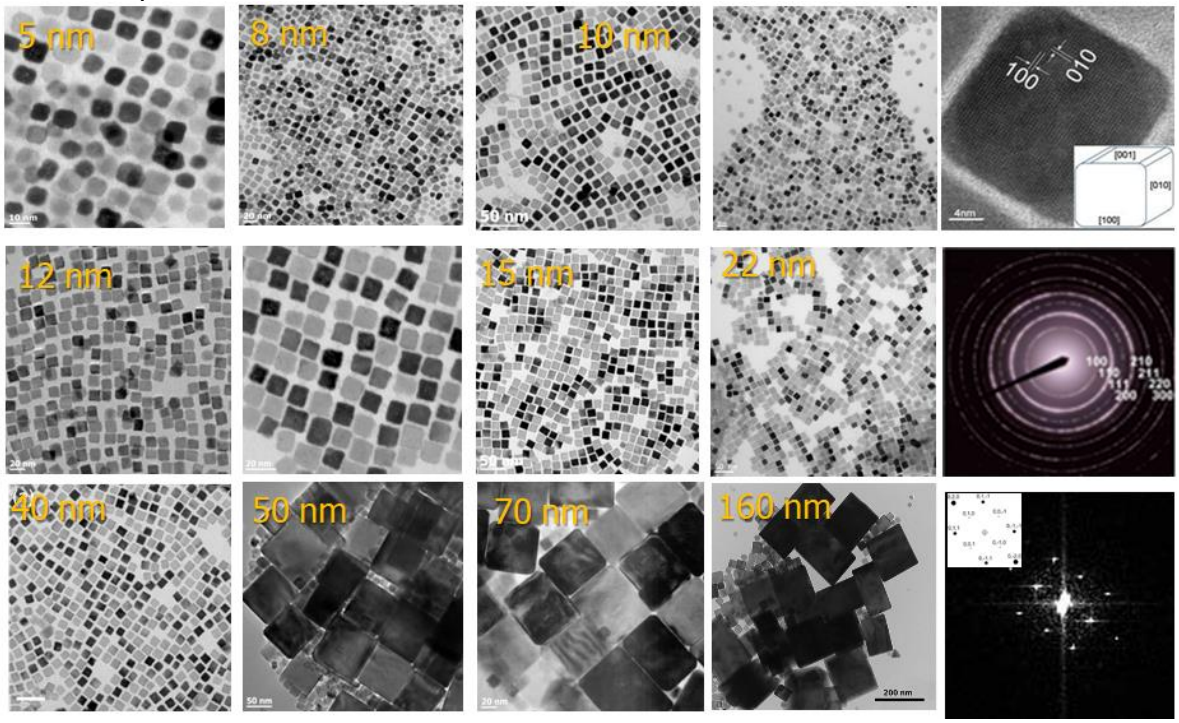

Figure 1. TEM micrographs of $BaTiO_3$ nanocubes synthesized at 180 ^oC by varying the polarity of the reaction medium and the reaction time (from 48 to 96 hours).

We have demonstrated that a rigorous control of the polarity of the solvent allows the stabilization of $BaTiO_3$ nanoparticles with a spherical and cubic shape. The optimum reaction temperature was identified as being 180 ^{o} C for the stabilization of $BaTiO_3$ cuboidal nanocrystals, while the varying the reaction time from 24 to 96 hours allowed us to control the size of these nanocubes in the range from 5 nm to 160 nm.

TEM images presented in Figure 1 reveal the morphology and crystallinity of $BaTiO_3$ nanocubes obtained under different reaction conditions. Nanocubes present an average edge length which can be varied from 5±1 nm to 160±2 nm, respectively and they are well separated due to the retention of capping agent molecules on their surfaces

Furthermore, through the subtle variation of the concentration ratio of oleic acid and the precursors, we managed to obtain variations from the cubic morphology of the nanoparticles, obtaining dodecahedron shaped nanoparticles (truncated nanoparticles).

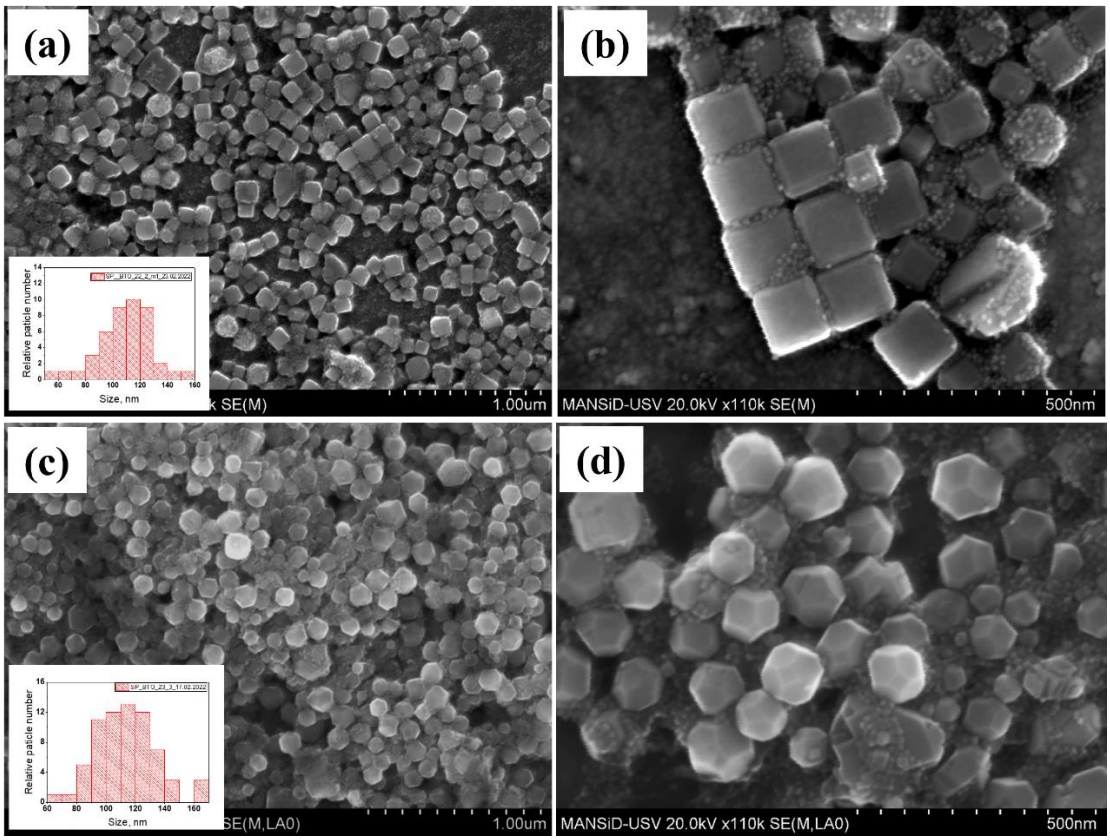

Figure 2. FE-SEM micrographs of $BaTiO_3$ with cubic (a-b) and dodecahedron (c-d) shape nanoparticles recorded with different magnitudes. The insets show the size histograms revealing a size distribution between 60-160 nm

To further increase the values of the dielectric constant of $BaTiO_3$ cuboidal nanocrystals **we doped them with rare earth ions**. Dielectric spectroscopy of the $Ba_{1-x}La_xTiO_3$ ($0.01 \leq x \leq 0.07$) nanocubes revealed values of the dielectric permittivity higher than that of the parent nanomaterial along with excellent $tan\delta$ values, which confirmed the incorporation of the Ln^{3+} ions under solvothermal conditions at low temperature. For example, at 1 kHz, the dielectric constant at room temperature for the pristine $BaTiO_3$ sample is ε=72 whereas the dielectric constant of the 1 mol % La-doped $BaTiO_3$ is ε=138, respectively. The loss tangent was found to decrease upon doping $BaTiO_3$ nanopowders with La^{3+} ions, which is in line with results reported by other groups in the case of rare earth doped $BaTO_3$ podwers. Additionally, piezoresponse force microscopy measurements performed on these nanocrystals showed that the permanent, reversibly switchable polarization observed in the parent material is preserved upon incorporation of the Ln^{3+} ions into the perovskite host crystal. The bandgap value of the $BaTiO_3$ colloidal nanocrystals decreased significantly upon incorporation of lanthanoid ions into the perovskite host lattice. These results have been published in ***CrystEngComm, 24 (2022) 7089-7102.***

III. 2. Fabrication of semiconducting and dielectric inks incorporating $BaTiO_3$ nanoparticles of different sizes. Characterization of their physico-chemical properties. The control of the surface composition of BaTiO3 nanocrystals and their dispersion in different solvents to obtain stable dielectric inks represents one of the most important results of this project because it allowed obtaining thin dielectric layers deposited on both rigid and flexible substrates. As-synthesized $BaTiO_3$ (BTO) nanocrystals with three different sizes: 12, 20 and 39 nm were passivated with both non-polar (oleic acid molecules) and polar (BF_4^- ions) ligands. By echanging the capping ligand via simple replacement reactions we demonstrated that the dispersibility of these colloidal nanocrystals can be tuned in both non-polar and polar solvents. Specifically, the passivation of the BTO nanocrystals with BF_4^- ions was achieved by replacing the oleic acid molecules on their surface with ions by treating with $NOBF_4$ in polar solvent solutions. $BaTiO_3$ nanocrystals passivated with oleic acid molecules are hydrophobic, being dispersible in non-polar solvents, such as toluene or hexane, with the formation of very stable colloidal solutions that can be kept for several years without the formation of sediment deposits. At the other end of the spectrum, nanoparticles passivated with BF_4^- ions are dispersible in polar solvents, such as acetone or dimethylformamide with the formation of stable colloidal solutions that can be used as dielectric or ferroelectric inks. Figure 3 shows the toluene solutions with 15 nm BaTiO3 nanocubes and the dimethformamide solution containing $NOBF_4$ before and after the ligand exchange process, as well as dielectric inks in toluene containing $BaTiO_3$ nanocubes with different concentrations, varying from 9, 75 to 150 mg of nanoparticles/ml of solvent.

Figure 3. Ligand exchange process between oleic acid and $NOBF_4$ and dielectric and ferroelectric inks with a different content of $BaTiO_3$ nanocubes.

III. 3. Dielectric characterization of differently-sized $BaTiO_3$ nanocrystals compacted in pellets via cold pressing and/or plasma sintering. The dielectric characterization of oxide nanopowders is a complicated and not yet rigorously solved problem. In general, the reliability of the dielectric characterization of powdered samples is questionable when this is performed by inserting the pelletized powder between two parallel plates in a capacitor geometry folowed by the measurement of the capacitance in the radio frequency domain, mostly because of the porosityof the powder. This means that the geometry of the system is not well defined, the electric field is not homogeneous inside the capacitor and the approximation of the planar capacitor parallel is no longer valid. In the case of a homogeneous dielectric, without porosity and inclusions, the field is uniform inside it and its value equal to the applied one (represented in green color in Fig. 4a), while for a dielectric with pores, or for a multiphase composite, the field becomes strongly inhomogeneous, with regions inside with a higher field value (red speckles in Fig. 4b), or a much smaller field value (blue in Figure 4b).

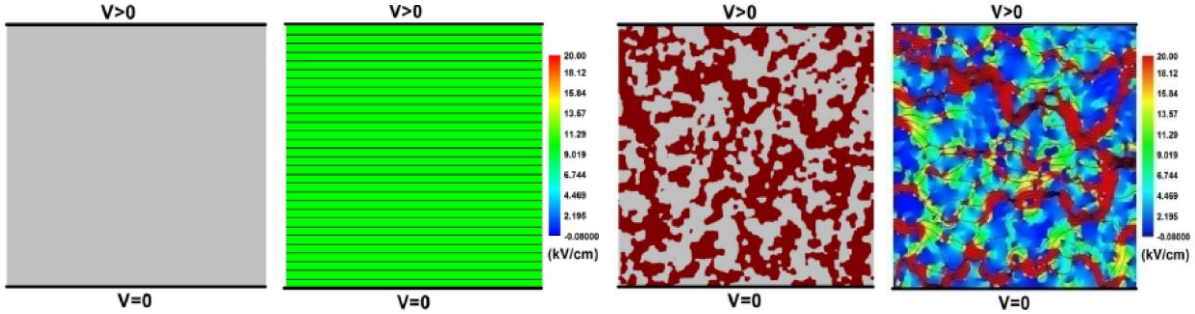

Figure 4. Cross-sectional distribution of the electric field calculated by using FEM in the case of : (a) a homogeneous dielectric: the field is uniform (green); (b) a composite with 50% dielectric with high permittivity and porosity: the field becomes inhomogeneous.

Besides the inhomogeneity of the field resulting from the porosity of the powder, an additional contribution to the dielectric properties is brought by interfaces. This contribution can surpass the volume contribution of the particles, thereby affecting substantially the calculated cvalue of the dielectric permittivity. Despite these limitations, there are still numerous publications that use this approach. Other methods have been proposed in the literature, such as the one based on the creation of nanoparticle suspensions either in liquid or in a solid polymer. Using variable concentrations and appropriate models, a value of the permittivity of the embedded particles can be extrapolated. In this project we developed a rigorous method for the measurement of the permittivity of ferroelectric nanoparticles by fabricating composites with different concentrations embedded in solid polymer, such as PVDF. Based on the effective dielectric permittivity measurements of these composites, of various concentrations, and numerical calculations using the finite element technique (FEM) developed previously by the UAIC group for different types of composites (Figure 5) and performing search algorithms (inverse problem), a value for the permittivity of ferroelectric nanopowders that represent a composite with f→100% can be extrapolated. Apart from the integration of ferroelectric nanoparticles in polymer matrix composites, another approach involved the sintering of these cubic $BaTiO_3$ nanoparticles in dense ceramics, using traditional sintering methods as well as plasma sintering (SPS). The goal was to fabricate dense $BaTiO_3$ structures with clearly defined boundaries and to investigate their functional properties.

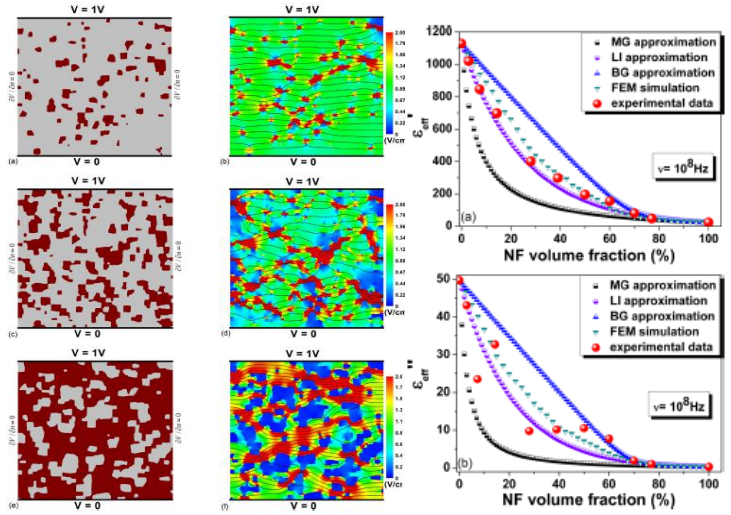

Figure 5. Composite microstructures, the calculation of the effective field inside the composite using FEM techniques and the effective permittivity in the composite depending on the concentration of the filler material.

Scale effects in ferroelectrics, especially in $BaTiO_3$, are a subject of great interest, as they are related to the current trend of miniaturization of components in microelectronics, particularly passive ones such as multilayer ceramic capacitors. The sharp decrease in permittivity in the case of ceramics with grain sizes below 100 nm was explained on the basis a series of effects: (a) intrinsic, related to the reduction of their ferroelectric character due to the decrease in the c/a tetragonality with decreasing grain size; (b) extrinsic, induced by the increase in the weight of intergranular boundaries related to the decrease in granulation. $BaTiO_3$ nanoparticles with cubic morphologies and average dimensions ranging from 5 to 25 nm range were sintered in a plasma arc (SPS) to densify the powders without grain growth, along with preserving the cubic shape, their nanoscale dimensions and phase purity (Figure 6).

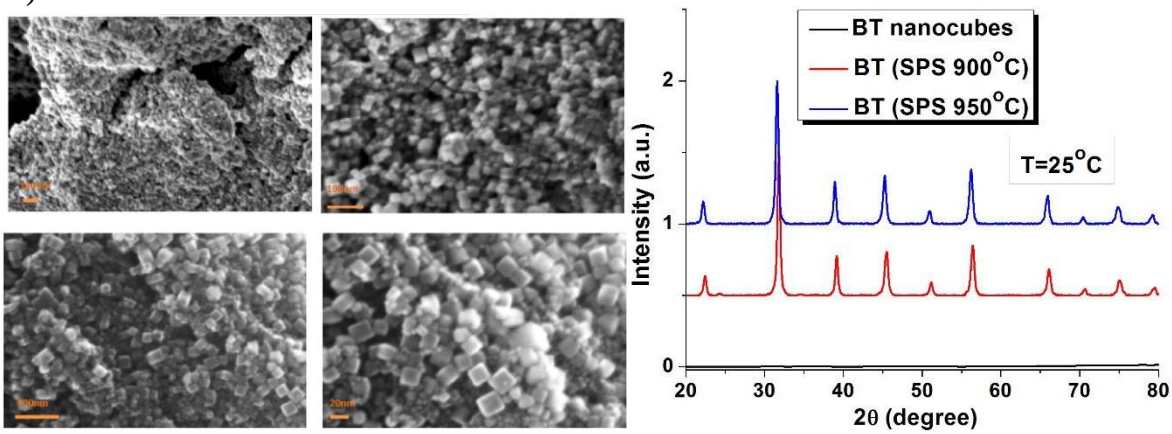

Figure 6. *SEM microstructures of $BaTiO_3$ with cubic morphology and the diffractograms of the powder and of the SPS sintered ceramics.*

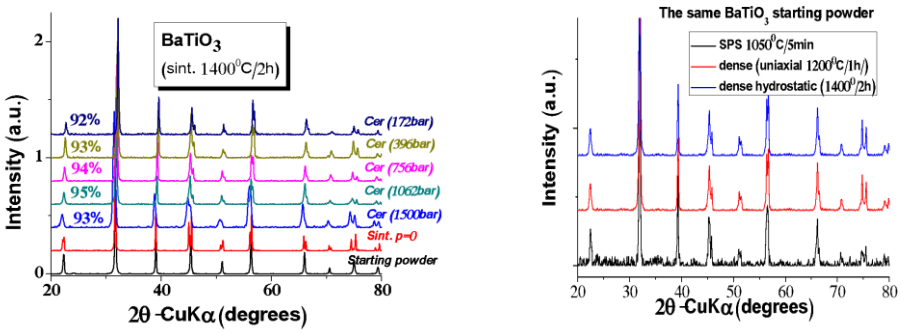

Figure 7. Diffractograms of $BaTiO_3$: (left) pressed at different pressures and traditionally sintered at 1400 °C/2h; (right) uniaxially pressed, hydrostatically and sintered by SPS or traditionally.

As granular interfaces are considered regions with defects, less ferroelectric, and therefore characterized by lower permittivity; the increase of their weight at a nanoscale level leads to an implicit decrease in permittivity, in accordance with the experimental results and calculations based on the "brick wall" model ("brick- layers").

Exploring novel experimental approaches to increase the the intergranular boundaries in powdered samples containing nanoparticles with the smallest dimensions can lead to the rational design of nanoceramics with very high values of the dielectric permittivity (> 1000). Moreover, the linear tunability of these nanostructured systems, as well as the higher breakdown field, can be useful characteristics for the applications of such ceramics in electrostatic energy storage. This aspect was analyzed in $BaTiO_3$ nanostructured ceramics. Thus, using cubic nanoparticles and appropriate sintering conditions, high densities (over 90%) and perfect intergranular boundaries in ceramics were expected to be obtained.

As a first test in this stage, pressing and sintering steps of commercial Sigma Aldrich 99.9% nanopowders (pseudocubic symmetry, d~60nm) were performed. Through all methods, acceptable densities of over 92% were obtained; the purity of the perovskite phase was maintained, as confirmed by X-ray diffractometry (Figure 7), and all samples are suitable for measurements for determining their dielectric properties. The dielectric properties were determined from the in plane-parallel geometry using both the Solatron 1260A impedance analyzer and the Hameg bridge. A protocol of measurements for the ceramic samples was devised. The effect density changing from 92% to 95% on the dielectric properties of two normally sintered ceramics, obtained from the same powder, can be inferred from the results displayed in Figure 8.

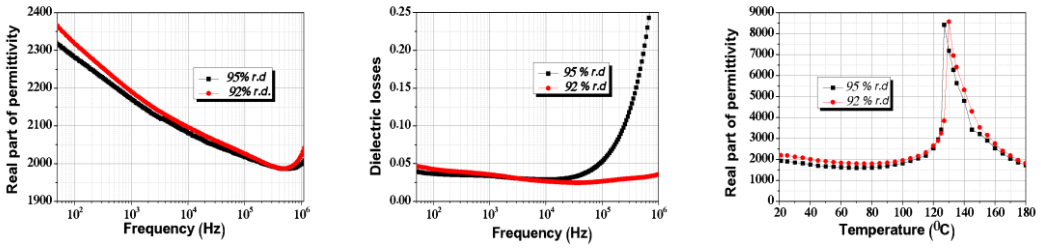

(a) (b) (c)

Figure 8. Dielectric properties of two ceramics with densities of 92% and 95% respectively: (a) permittivity vs. frequency at room temperature; (b) dielectric losses vs. frequency at room temperature; (c) permittivity vs. temperature at a frequency of 1kHz.

The values of the permittivity and losses at room temperature are similar, except for very low and high frequencies. The permittivity decreases monotonically with the increase in frequency up to 0.5 MHz after which there is an increase related to the increase in losses as well (Figure 8a,b). There is a slight difference in the values of the permittivity and its maximum between the two samples (Fig. 8c). It is known that in ferroelectrics, unlike ordinary dielectrics, the polarization is a nonlinear function of the electric and thermal fields. Most studies on the dielectric changes of thin films are carried out with an external electric and thermal field.

III. 4. Structural characterization of differently-sized $BaTiO_3$ nanostructures by Powder X-ray Diffraction, Vibrational Spectroscopy (FTIR), Transmission Electron Microscopy (TEM) and Scanning Electron Microscopy (SEM). Structural characterization by X-ray diffraction of thin layers obtained from dielectric colloidal nanoparticles. Characterization of the electrical properties, in variable temperature, of the obtained thin layers. Determination of thermal activation energies of electrical conductivity.

The influence of molecular or inorganic species, used to passivate the surface of the $BaTiO_3$ nanocubes, on their crystalline structure was the subject of a systematic study using advanced characterization techniques were used, including neutron diffraction combined with pair distribution function (PDF) analysis and ab initio molecular dynamics. This analysis is key to confirm the stabilization of the tetragonal crystalline structure at ambient temperature, the structure that corresponds to the existence of ferroelectric properties in nanocubes and, implicitly, to high values of the dielectric constant. Such a study is required for at least two reasons: (1) the effect of the ligand molecules passivating the surface of the perovskite oxide nanocrystals on their polarization and ferroelectric properties is largely unexplored and (2) the passivation of the nanocrystal surfaces is critical for the fabrication of inks dielectric and ferroelectric inks containing nanocrystals, inks which will be used in creating of thin dielectric layers for the design of flexible electronic circuitry, such as capacitors and field effect transistors.

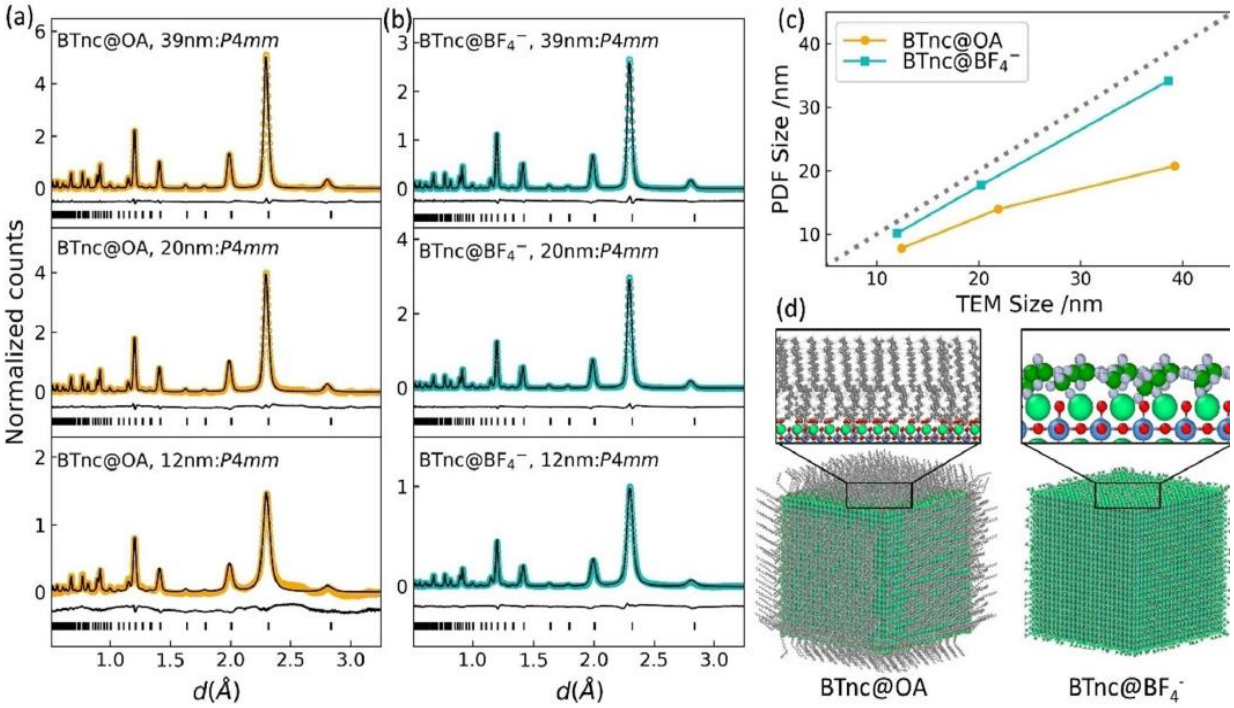

Figure 9. Rietveld analysis of neutron diffractograms of powders formed from different sizes $BaTiO_3$ passivated with oleic acid molecules (a) and, respectively, BF_4 (b). The experimental data is represented by orange and blue circles, while the black lines represent the simulated neutron diffractogram and the gray lines represent the difference between the experimental data and the simulated diffractograms; c) The size of the nanoparticles determined by electron microscopy compared with the size obtained by structural refinement; d) Atomistic models that describe the distribution of ligands on the surface of nanoparticles

In this study, we used $BaTiO_3$ nanocrystals with three different sizes: 12, 20 and 39 nm passivated with both non-polar (oleic acid molecules) and polar (BF_4^- ions). The passivation of nanocrystals with BF_4^- was achieved by replacing the oleic acid molecules on their surface with ions upon treating toluene solutions of $BaTiO_3$ nanocrystals with with $NOBF_4$ dissolved in polar solvent. As can be seen from Figures 10a and 10b, the neutron diffraction patterns of differently-sized $BaTiO_3$ passivated with oleic acid molecules or BF_4^--ions were indexed using tetragonal symmetry (space group *P4mm*). It should be noted that in the case of the smallest nanoparticles (12 nm) the difference between the tetragonal and the cubic model used in the refinement of structures by the Rietveld method is very small, the values of the GOF (goodness of fit) R_{wp} parameters being 0.882 (for the nanoparticles of $BaTiO_3$ passivated with oleic acid molecules) and 2.035 (for $BaTiO_3$ passivated with BF_4^-) in the case of using tetragonal symmetry (space group *P4mm*) and, respectively, R_{wp}=0.886 (for $BaTiO_3$ passivated with oleic acid molecules) and 2.059 (for $BaTiO_3$

passivated with BF_4^-) in the case of using cubic symmetry (space group *Pm3m*). The structural refinement of these nanopowders was carried out using structural models corresponding to an orthorhombic and rhombohedral symmetry, given the fact that $BaTiO_3$ shows three structural transitions with decreasing temperature, from a cubic symmetry to a tetragonal one (at T= 120°C), then orthorhombic (at T= 0°C), and respectively rhombohedral (at T= -90°C). The results of the structural refinement of $BaTiO_3$ using the 4 models show that, in the case of small-sized nanoparticles, the broadening of the diffraction peaks due to the small size of the crystallites makes the distinction of the type of structure inconclusive by using the structural refinement of the Rietveld method, as the only experimental method of identifying the structure of these nanocrystals. As can be seen from Figure 9c, the size of the nanoparticles calculated in the case of the cubic structure from the pair distribution function (PDF) differs significantly from the size of the nanoparticles determined experimentally by electron microscopy. For this reason, the neutron diffraction data were supplemented with data obtained from structural analysis using the pair distribution function (PDF) corresponding to the different possible types of symmetry (cubic, tetragonal, orthorhombic and rhombohedral). The results obtained by this method are presented in Figure 10.

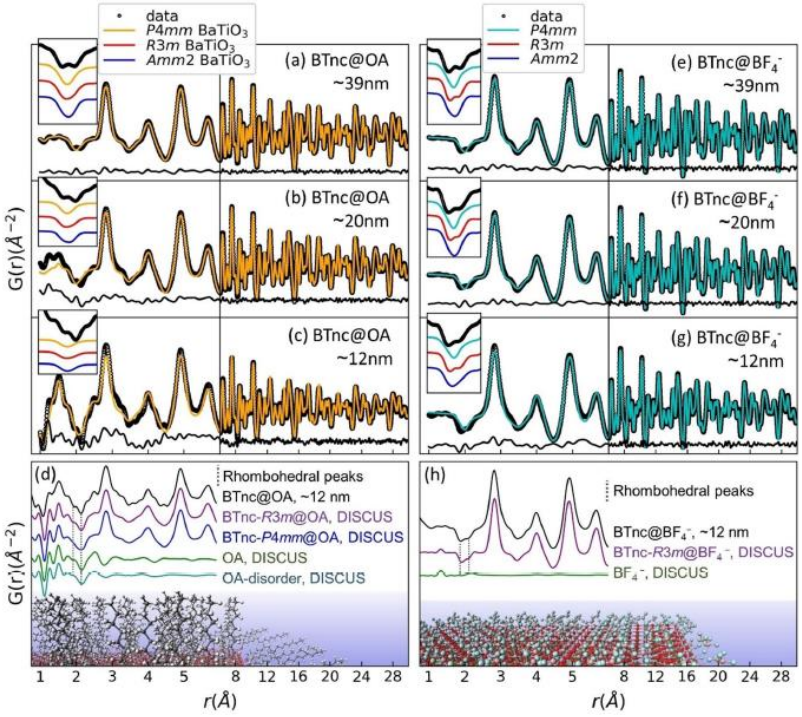

Figure 10. Analysis of the pair distribution function (PDF) corresponding to the neutron diffractograms for $BaTiO_3$ passivated with oleic acid molecules (BTnc@OA) and BF_4^- (NTnc@BF_4^-)

It is interesting to note that in the case of $BaTiO_3$ with a size of 12 nm, the structural model that led to values closest to the experimental results is the orthorhombic (space group Amm2) in the spatial domain above 30 Å, with similar results in the case of the rhombohedral and tetragonal models. This study also allowed us to answer another fundamental question related to the crystalline structure of $BaTiO_3$, namely "what is the length scale at which this rhombohedral structural modification is present in the perovskite type nanoparticles and, if so, how is this structural disorder influenced by the species that passivate the surface of the nanoparticles?" From the examination of the value differences of the crystal structure parameters of the 12 nm $BaTiO_3$ using different structural models (tetragonal and rhombohedral, Figure 11a; and orthorhombic and rhombohedral, respectively,) it was found that, in the case of $BaTiO_3$ mono-block rhombohedral structure (space group *R3m*) the fit is acceptable at distances of maximum 9 Å (approximately two elementary cells), which is in agreement with the value of 10 Å, a value that corresponds to the coherence length of the local rhombohedral distortion associated with the phase transition (order-disorder) in the case of the $BaTiO_3$ described in the specialized literature. The difference between the calculated R_{wp} confirms the fact that the tetragonal structural model (space group *P4mm*) best describes the crystalline structure of $BaTiO_3$ for long coherence lengths, as it was expected. At the same time, it is observed that the rhombohedral structural model best describes the local structure of $BaTiO_3$ in nanocrystalline form, which suggests that in the case of nanoparticles their size stabilizes the dipole-dipole correlations, resulting in an orthorhombic type coherence in the case of distances intermediate (of the order of a few nanometers).

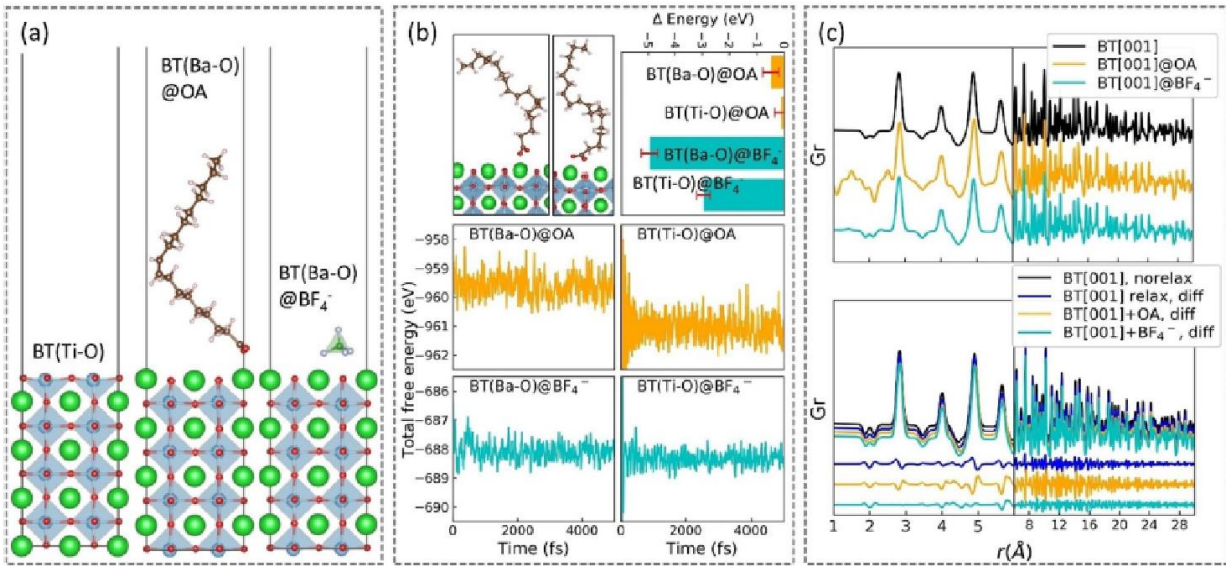

Figure 11.Results obtained using DFT for: a) a $BaTiO_3$ block with a rhombohedral structure terminated by a TiO surface (left), oleic acid molecules (middle) and BF_4^- (right) terminated by -a BaO surface. b) Oleic acid molecules absorbed on the TiO and BaO surfaces of a $BaTiO_3$ and the corresponding free energies at 300 K for different configurations. c) Neutron diffractograms obtained from the optimized DFT structures.

The results obtained in the case of $BaTiO_3$ with a size of 12 nm show that the rhombohedral model (space group *R3m*) describes the corresponding crystalline structure at a distance of approximately 25 Å in real space if they are passivated with BF_4^- (being polar), while for nanoparticles passivated with oleic acid, this distance is only 10 Å. The difference of approximately 4.5 nm between the values of the size of the shape function suggests that the inert dielectric layer ("dielectric dead layer") on the surface of the nanocubes is approximately 2 nm in the case of nanocubes passivated with oleic acid molecules and practically non-existent in the case of passivated nanocubes with BF_4^- , which was experimentally confirmed by the existence of a more robust ferroelectric behavior in the case of polar $BaTiO_3$. Similar results were also obtained in the case of larger $BaTiO_3$ (20 and 39 nm), in which case the nanoparticles passivated with oleic acid molecules have a lower correlation length of 3.7 and, respectively, 14 nm than those passivated with BF_4^-. From the calculated form of the pair distribution function PDF (Figure 11c) obtained using the density functional theory (DFT), it can be seen that the difference in the case of oleic acid molecules is greater than that observed in the case of the surfaces of the nanoparticles of $BaTiO_3$ unpassivated. This suggests that local structural distortions are observable in the case of $BaTiO_3$ whose surface is passivated with non-polar species, such as oleic acid molecules. Similarly, the energy corresponding to BF_4^- is lower than that observed in the case of unpassivated $BaTiO_3$, as well as oleic acid molecules, which confirms once again that polar BF_4^- contribute to the increase stability of the local rhombohedral structure on the nanoparticle surface, in accordance with the results obtained from neutron scattering analysis. This component of the project was developed with the help our collaborator Prof. Katharine Page from the University of Tennessee (USA) and the Oak Ridge National Laboratory (USA), which allowed us access to the neutron source in order to perform neutron diffraction measurements and "pair distribution function" analysis.

Verification of the morphological characteristics and mechanical properties, using atomic force microscopy (AFM) and the Scotch method, for the thin layers obtained from dielectric nanocrystals

The morphology of the $BaTiO_3$ thin layers fabricated by depositing solutions containing 15 nm $BaTiO_3$ particles together with their piezoelectric response were studied using atomic force microscopy (AFM) and piezoresponse force microscopy (PFM) at ambient temperature. Figure 12 shows images obtained by these microscopic techniques for a 300 nm thin layer deposited on a polyimide substrate. It can be seen that the thin layer is uniform and has no roughness or defects, such as cracks or voids; the constituting nanocubes of clearly visible.

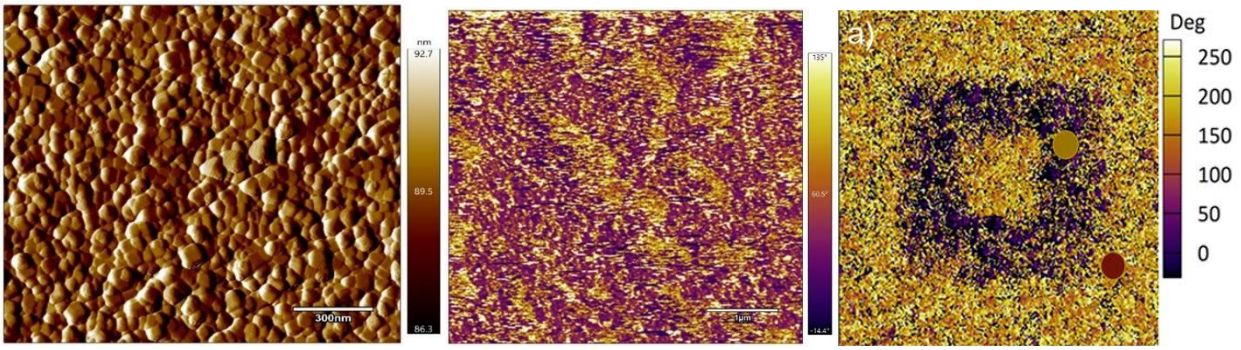

Figure 12. Atomic force microscopy images (left) of a 300-nm-thick thin layer deposited from a solution of 15-nm $BaTiO_3$ in toluene and the piezoelectric response of this film (center). Right: PFM image of the thin layer subjected to the action of an electric field with diametrically opposite orientations, showing the orientation of the electric dipoles in $BaTiO_3$ according to the applied electric field.

The piezoelectric response of this thin layer in the presence of an electric field appears as a map with yellow and purple regions (false colors), which correspond to the „up" and „down" orientation of the electric dipoles, thereby confirming that the thin layer is ferroelectric at ambient temperature. Moreover, the thin layer was placed in contact with a very sharp electrode ("tip") through which a voltage +20 V bias was applied, causing the upwards orientation of the electric dipoles. These areas appear in the corresponding PFM image (Figure 12 middle) in orange color. The electrode was later withdrawn and the polarity of the current was reversed followed by making contact with the thin layer on selected regions of the thin layer, leading to a reversal of their orientation (downwards), these areas appearing in the PFM images in purple color. The piezolectric response results of the $BaTiO_3$ nanocubes films indicate that they can be successfully used to physically encode information in the form of "0" and "1" using conventional Boolean algebra.

III. 5. Fabrication of Dielectric Layers by Using Solutions of Colloidal $BaTiO_3$ Nanocrystals and their Characterization

In the first two years of the project, the research activities of the USV and UAIC teams related to Task 2 were focused to the design of novel polymer-ceramic nanocomposite films by using different types of polymers, whereas the NIMP partner was involved in the structural characterization of such composite materials. The rationale used to select the polymers was their polar/non-polar character, which should be similar that of the dielectric/ferroelectric nanocrystals, their solution processability and the relative higher value of their dielectric constant. The best composite structures in terms of filler homogeneity, absence of pinholes and agglomeration into the polymeric matrix, flexibility, smooth surfaces, reduced porosity, increased permittivity, and low dielectric losses have been used to fabricate flexible capacitors and FET prototypes, whose electrical performance have been tested and continuously optimized.

Polymer–ceramic nanocomposite films consisting of titanate perovskite nanoparticles dispersed into a polymer matrix (0–3 composites) have garnered increasing interest due to their superior performance characteristics, which can be used in flexible modern electronics and energy storage systems. Our first work reported on the rational design of substrate-free polymer ceramic nanocomposite films consisting of differently sized (10 nm and 20 nm), oleic acid-coated $BaTiO_3$ colloidal nanocrystals dispersed into styrene butadiene styrene (SBS) by using a highly reliable solution-based method. The amount of filler nanoparticles was varied from 0 to 50 wt.% and the resulting films preserved their original mechanical properties, without signs of brittleness or defects. The effect of the size and weight fraction of the filler nanoparticles on the morphology and the dielectric properties of the BTO–SBS nanocomposite films was systematically investigated. Electron microscopy images showed that the filler nanoparticles are uniformly distributed within the SBS matrix with a substantial decrease of the interparticle distance within the elastomer matrix when the filler content was varied from 10 to 50 wt.% (Figure 13).

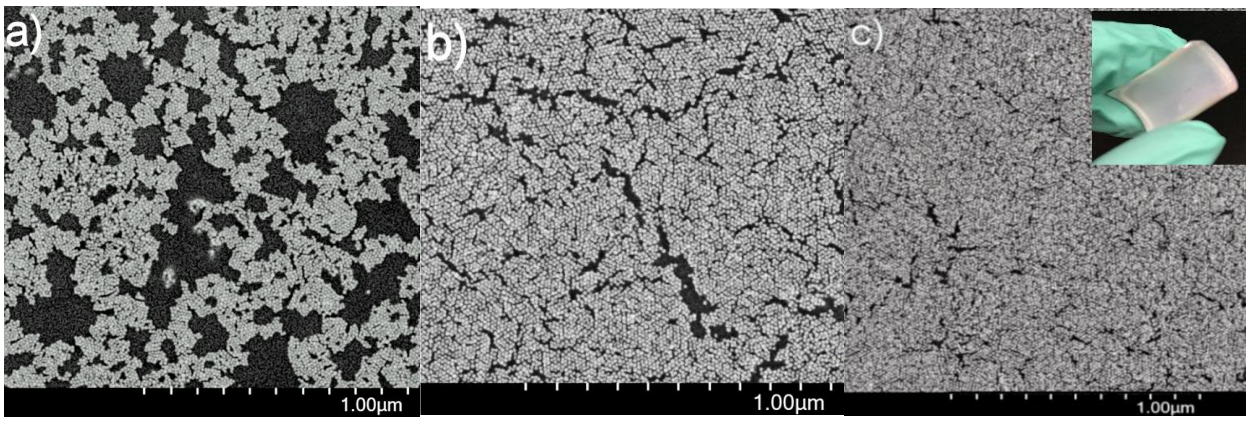

Figure 13. Surface field emission scanning electron microscopy micrographs of BaTiO–SBS nanocomposite films with a content of 30% (a); 40% (b) and 50% (c) 10 nm BaTiO3 colloidal nanocrystals as ceramic fillers.

The morphology and surface topology of the BTO-SBS nanocomposite films obtained by incorporating 10 nm $BaTiO_3$ nanocubes into the elastomer matrix have been investigated by atomic force microscopy (AFM), the corresponding images being presented in Figure 14. The images clearly show that the nanocomposite films are uniform and possess a roughness that changed from 3.0 nm for the neat SBS polymer to 32.5 nm for the (50 % wt.) BTO-SBS nanocomposite film for a raster scanned area of 5 μm^2. Room temperature dielectric spectroscopy data (Figure 15) showed that the dielectric constant of the SBS elastomer improved significantly (from ε=4 to ε=34.3 and ε=33.7 upon incorporating 10 nm and 20 nm $BaTiO_3$ nanocubes). The breakdown field values were found to decrease from 195 kV/cm^{-1} for the neat elastomer to 15 kV cm−1 for the SBS–BTO nanocomposite films with 50% (wt.) filler nanoparticles. As shown in Figures 15a and 15c, the real part of the dielectric constant of BTO-SBS nanocomposite film containing 10 nm and 20 nm $BaTiO_3$ nanocubes dispersed into the elastomer matrix with concentrations of the filler nanoparticles in the range from 10 to 50 % showed a weak dielectric dispersion in the whole frequency range (from 100 Hz to 1 MHz) which makes these nanocomposite materials attractive for high frequency applications. Specifically, the dielectric constant of BTO-SBS nanocomposite films containing 10 nm $BaTiO_3$ nanocubes with a filler concentration ranging from 10 to 50 wt. % was found to decrease by 3.13 % and 6.69 % in the frequency range from 100 Hz to 1 MHz, whereas for 20 nm nanocubes this decrease was by 1.42 % and 7.11 % for the same filler concentration and frequency range, respectively. The decrease of the dielectric constant values with the frequency has been ascribed to the dielectric relaxation of the $BaTiO_3$ nanoparticles and the existence of interfaces due to the uniform dispersion of the filler nanocrystals within the elastomer matrix. Also, at high frequencies, there is a lag time between the field reversal and the reorientation of the dipoles, which leads to a decrease of the value of the dielectric constant due to the relaxation of electrical dipoles.

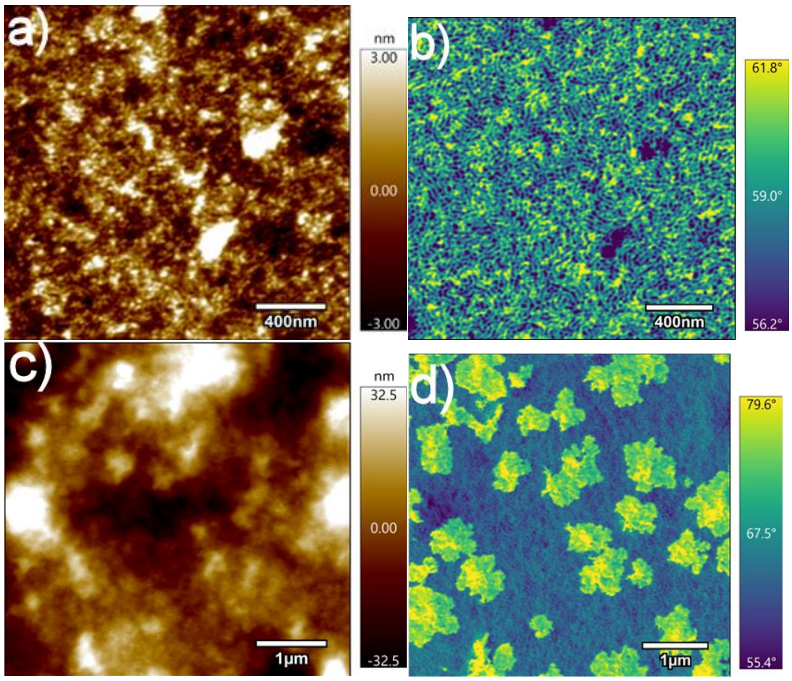

Figure 14. Atomic force microscopy images of the neat SBS film (a) and a (50% wt.) BTO-SBS nanocomposite film.

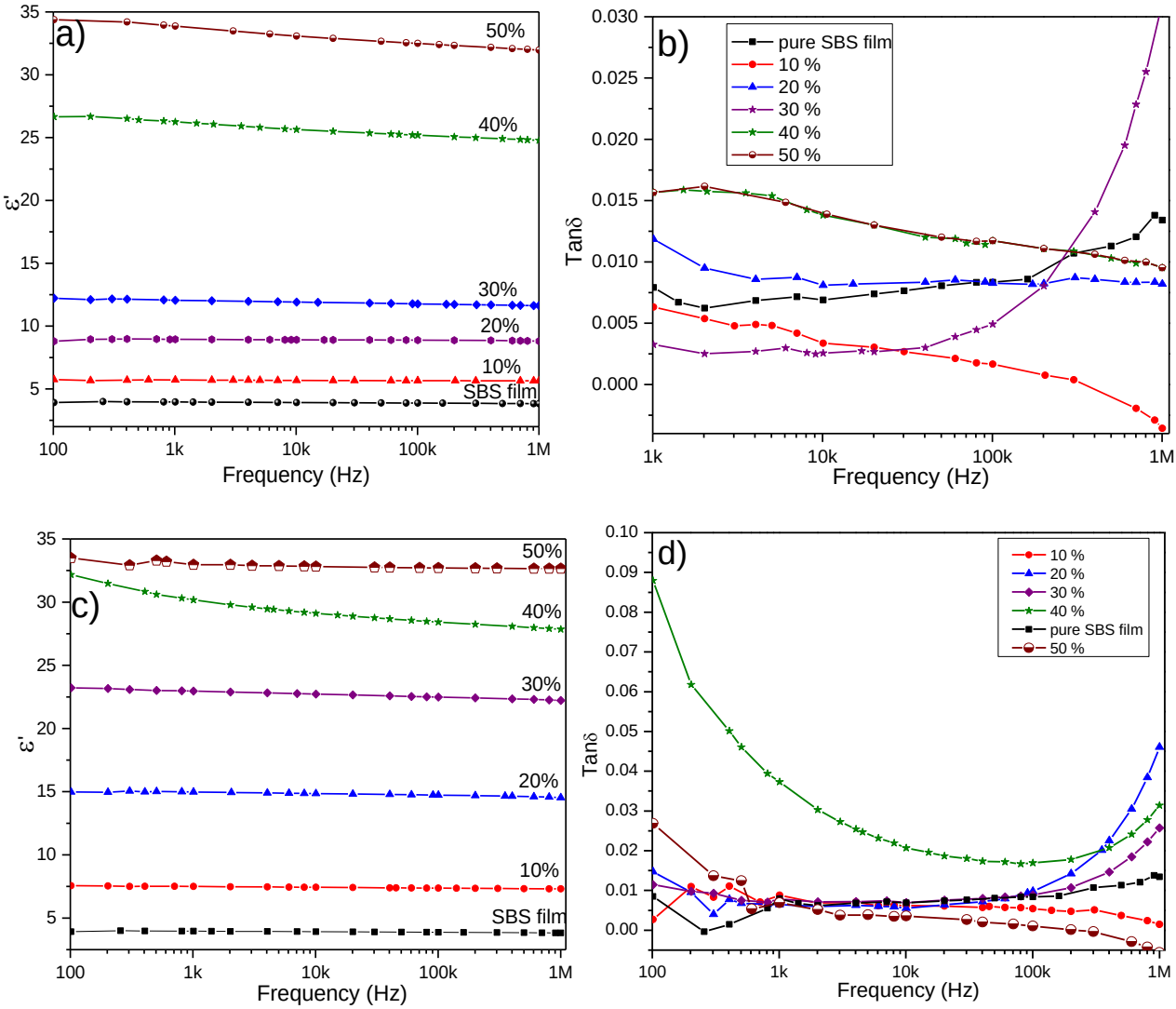

Figure 15. Frequency dependence of the relative dielectric constant (ε') and loss tangent of BTO–SBS nanocomposite films made by using 10 nm (Fig. 19a and b) and 20 nm (Fig. 19c and d) $BaTiO_3$ nanocubes. The concentration of the filler nanoparticles ranged between 0 and 40 wt. %, respectively.

The experimental results show that these BTO–SBS nanocomposite thin films exhibit superior properties, which make them attractive for implementation in high-performance capacitive storage devices, wearable technology, sensors and nanoelectronics. We show that the BTO–SBS nanocomposite films fabricated by the proposed approach present high permittivity values along with excellent mechanical properties and can be potentially used in energy storage applications. *The results were published (grant members underlined) in a Q1 journal: D. Caruntu, B. Kavey, S. Paul, A.C. Bas, A. Rotaru, G. Caruntu, "Dielectric properties of solution-processed $BaTiO_3$–styrene butadiene styrene nanocomposite films", CrystEngComm*, **2020**, *22 1261-1272.*

A series of flexible composites based on $BaTiO_3$ nanocube-like fillers (with an average particle size of 15 nm) produced by USV whose microstructure was characterizd by NIMP were embedded in polymer matrices as PVDF, epoxy resin or gelatin biopolymer via solution casting by UAIC. Their electrical properties were compared with those of similar composites in which spherical BT particles with the same average particle size were used as filler to observe the role played by the cubic shape on the electrical properties (related to possible electric field enhancement in sharp regions). The structural, microstructural, dielectric, ferroelectric and piezoelectric properties of such composites have been investigated by the UAIC team . Three types of polymers have been tested as matrix: (i) epoxy resin, (ii) polyvinylidene fluoride – PVDF and (iv) gelatin bio-polymer, respectively.

The studies on epoxy- $BaTiO_3$ composites showed an increase of the permittivity upon increasing the amount of $BaTiO_3$ nanoparticles (almost twice higher in 5 wt.% $BaTiO_3$ compared to that of the epoxy matrix). These results also showed room temperature losses below 6% in the investigated radiofrequency

range. The *ac* conductivity linearly increased in log-log scale for frequencies above 100 Hz and did not show any significant relaxations. The *ac* resistivity ranges between $3x10^9$ Ω/m and 10^{11} Ω/m. However, for high $BaTiO_3$ contents the porosity was not controlled, and permittivity becomes even lower than in pure epoxy (Figure 16), this indicating that the homogenization of these composites should be further optimized and solvent evaporation during co-polymerization of epoxy bicomponent should be better controlled in the next steps.

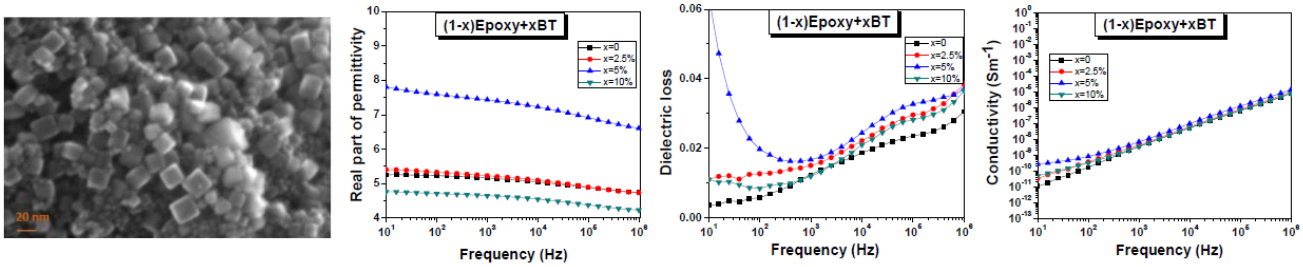

Figure 16. SEM micrographs of starting $BaTiO_3$ nanocubes used for preparing polymer-based composites; permittivity, dielectric loss and ac conductivity vs. frequency for $BaTiO_3$ -epoxy composites.

(ii) All attempts to prepare composites by using $BaTiO_3$ with different shapes (nanocubes and spherical nanoparticles) or other nanoparticles embedded into the PVDF ferroelectric matrix have shown the *limitation of solution-based methods in eliminating the porosity* in this type of materials. As such, the further optimization of the preparation of these nanocomposites using PVDF are required. Better densities were obtained from experiments on flexible PVDF films by using larger particles (*e.g.*, micron $Ba_{12}Fe_{28}Ti_{15}O_{84}$), since these particles can be better isolated and dispersed within the polymer matrix leading to a better densification of the samples. The composites retain their flexibility to filler contents up to 9 wt.% and have shown a multifunctional character: dual magneto-piezoelectric response with a reasonable dielectric, ferro/piezoelectric and soft magnetic character, while maintaining a high flexibility. *These results were published in a Q2 journal (grant members underlined): F. Gheorghiu, <u>R. Stanculescu</u>, <u>L. Curecheriu</u>, E. Brunengo, P. Stagnaro, V. Tiron, P. Postolache, M.T. Buscaglia, <u>L. Mitoseriu</u>, PVDF–ferrite composites with dual magneto-piezoelectric response for flexible electronics applications: synthesis and functional properties, J. Mater. Sci. 55, 3926–3939 (2020)* An alternate way to decrease the porosity in PVDF-BT nanocomposites was also explored by an external collaboration by using a solvent-free method, *i.e.* by hot-molding (which is a technique not available in our group of partners). By this method, the successful densification to 100% of $BaTiO_3$-PVDF composites could be achieved, study which resulted in a publication, in which the contribution of the UAIC team consisted in the full electrical characterization of such PVDF- $BaTiO_3$ composites. *These results were published in a Q2 journal (grant members underlined): E. Brunengo, L. Conzatti, I. Schizzi, M.T. Buscaglia, G. Canu, L. Curecheriu, C.*

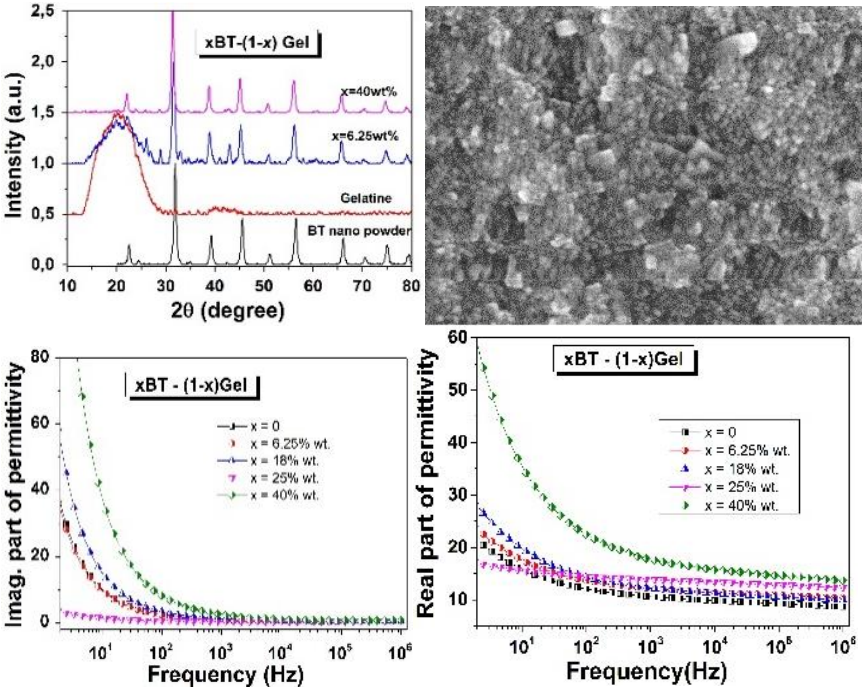

Figure. 17. XRD patterns of x $BaTiO_3$-(1-x)Gel thick films and microstructure for x=40% wt. Room temperature dielectric characteristics *vs.* frequency for x $BaTiO_3$-(1-*x*)Gel (*x*=0, 6.25, 18, 25 and 40. wt. %).

Costa, M. Castellano, L. Mitoseriu, P. Stagnaro, V. Buscaglia, Improved dielectric properties of poly(vinylidene fluoride)-$BaTiO_3$ composites by solvent-free processing, J. Appl. Polym. Sci. 138, 12, 50049 (2021)

(iii) Promising results in terms of processing flexible composites (*i.e.* a better densification, homogeneous distribution of filler nanoparticles) were realized by UAIC using a gelatin biopolymer as matrix with optimized $BaTiO_3$ nanocube fillers produced by USV. Gelatin is a natural protein-based compound derived by partial hydrolysis of native collagen existing in skin, tendons and bones of animals and is a very interesting material as matrix for non-toxic "green electronics" (bio-degradable, recyclable and bio-compatible). Gelatin is a polar polymer showing electroactive properties and has potential in integrated optical and electrical devices. By using a solvent-based method, flexible thick films x$BaTiO_3$-(1-x)gel with compositions x=0, 6.25, 18, 25 and 40 wt. % were obtained with a rather homogeneous dispersion of $BaTiO_3$ nanocubes within the matrix volume. The room temperature dielectric characterization in the frequency range ν=1-10^6 Hz indicated a slight increase of permittivity due to the $BaTiO_3$ nanoparticles addition from 9 (x=0 wt. %) to 15 (x=40 wt. %) at 10^5 Hz and low dielectric losses ~ 3-5 %, indicating good dielectric properties. Strong Maxwell-Wagner relaxations due to space charge effect at multiple $BaTiO_3$-polymer interfaces were observed experimentally below 100 Hz in all composites and mostly for ones with high $BaTiO_3$ contents, whereby the permittivity reached values as high as 50-60 (for x=40 wt. %) at 10 Hz compared to 20 (for x=0 wt. %), although high resistive losses were observed in these samples.

III. 6. Integration of thin dielectric layers in flexible capacitors and optimization of their performances)

Further, the room temperature dependence of the polarization *vs.* field dependences P(E) was investigated at different frequencies and the results for f=100 Hz are comparatively shown in Figure 18.

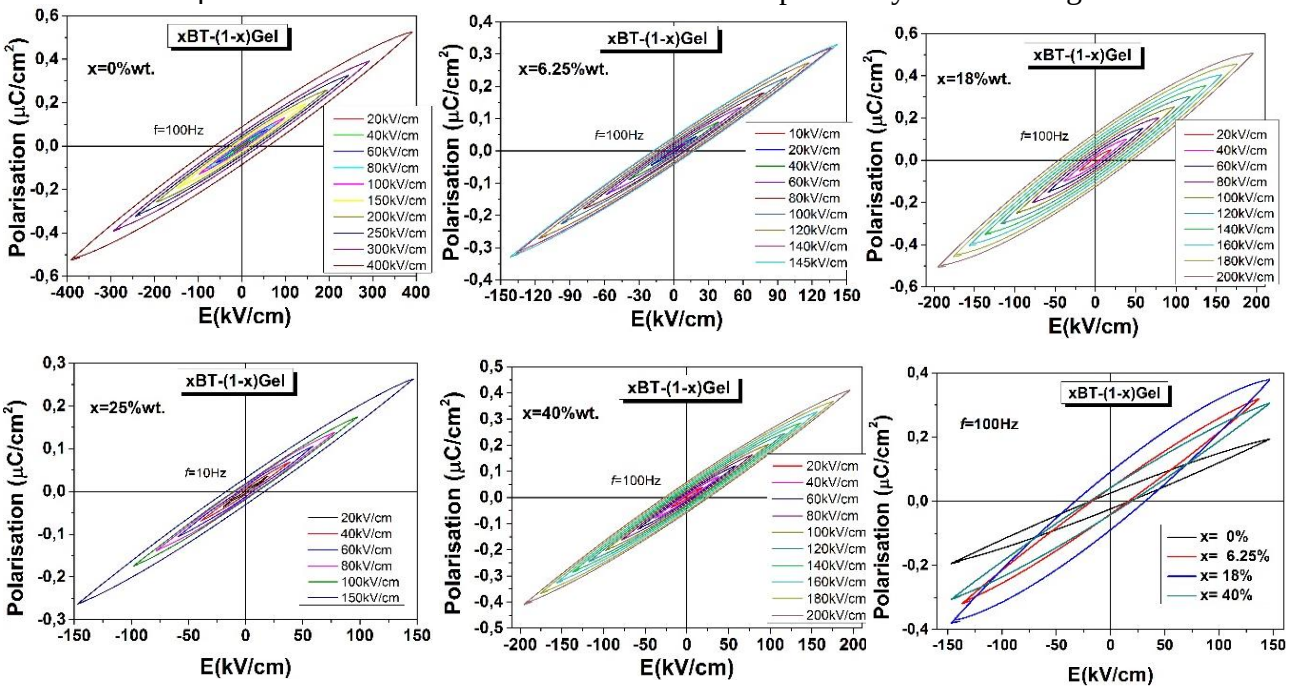

Figure 18. P(E) minor loops at f=100 Hz for x $BaTiO_3$-(1-*x*)Gel flexible composite films (*x*=0, 6.25, 18, 25 and 40 wt. %)

Together with the dielectric permittivity, the polarization increases with the addition of $BaTiO_3$ nanoparticles; however but for values of the electric field below the breakdown, a linear dielectric character was observed (equivalent with an RC group). The recovered energy density (W_{rec}) and stored energy density (W_{stored}) in the volume unit were determined from the *P(E)* loops (Figure 18) for fields in the range ($-E_{max}$, $+E_{max}$) by using the formulas:

$$W_{rec} = \int_{P_r}^{P_{max}} EdP \qquad W_{stored} = \int_{P_{-r}}^{P_{max}} EdP$$

and the energy storing efficiency is: $\eta = \frac{W_{rec}}{W_{stored}}\ x\ 100\%$, where: $W_{stored} = W_{rec} + W_{loss}$.

Among this series of flexible composites, x=18 wt. % shows the highest stored energy density of 36 mJ/cm^3, but its efficiency is 50 %, while the highest efficiency of 70% is found for x=6.25% with a stored energy density of 25.3 mJ/cm^3. The values are very low with respect to the best ones reported in literature for similar composites [S. Luo *et al.*, *Adv. Energy Mater*. **2018**, *9(5)*, 1803204], but they are still promising by considering the low level of the applied maximum field.

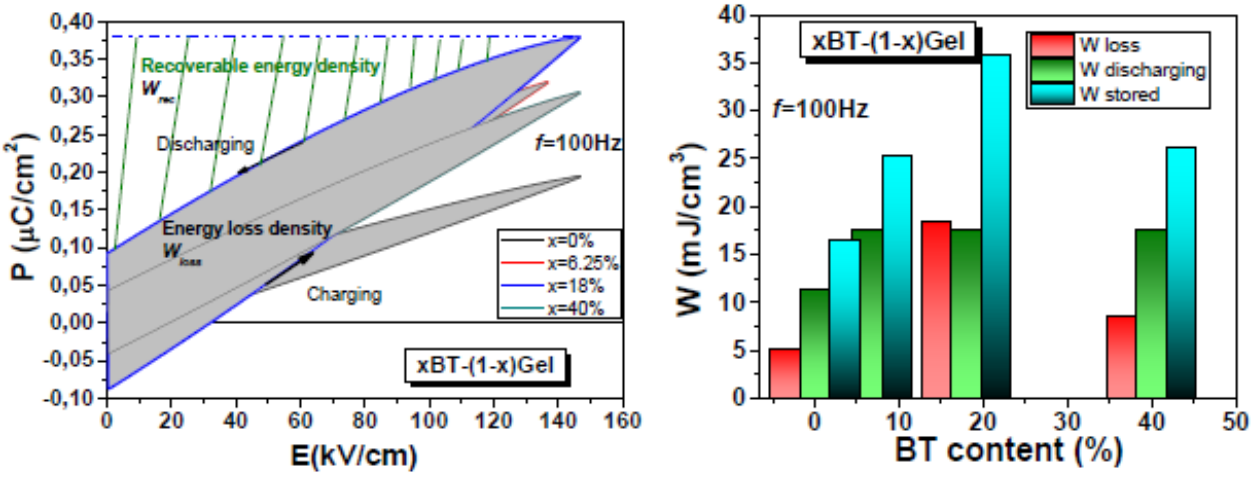

Figure 19. P(E) loops; loss, discharging and stored energy density for x $BaTiO_3$-(1-x) gel.

The attempts to increase the permittivity in flexible polymer-based composites by using $BaTiO_3$ *nanocubes combined with various polymer matrices resulted in a modest permittivity rise (about 2-3 times) compared to those of the pure polymers, presumably due to several factors:*

- The inherent porosity in composites processed by solution casting. The porosity is detrimental not only because it reduces the permittivity enhancement induced by the presence of the filler, but also because limits the maximum applied voltage by reducing the breakdown field. Increasing the filler composition above 40 wt. % would strongly reduce the flexibility of the composites. A further optimization of the processing parameters should be performed to enhance the energy storage ability of these materials;
- Due to the existence of surface effects, ultrafine $BaTiO_3$ nanoparticles have small permittivity and polarization values compared to their micron-sized counterparts. As such, cube-like particles with larger grain sizes should be further employed to increase more the composites permittivity. However, coarse grained particles limit the solution-based processability of such composites and their flexibility; therefore a balance between these two effects should be achieved to optimize the properties of the polymer-ceramic composites.
- A promising solution to maintain the flexibility and further increase the permittivity of these composites consists of embedding ultrafine metallic nanoparticles into $BaTiO_3$ -polymer composites

Integration of thin dielectric layers in flexible capacitors and optimization of their performances - Modeling.

In parallel with the experimental work aimed at the fabrication of polymer-based $BaTiO_3$ nanocomposites, we developed a theoretical modeling-based estimation of the influence of fillers with higher permittivity into a low permittivity polymer matrix on the dielectric properties of the nanocomposite. To this end, simulations were performed by using Finite Element Methods (FEM) applied to composites formed by a low-permittivity polymer matrix with ferroelectric nanoparticles as fillers (*e.g.* $BaTiO_3$). In the first step, the influence of the filler particles shape on the dielectric properties of composites for the same concentration was investigated. Numerical methods developed by the UAIC group were experimentally validated for the case of other inhomogeneous dielectrics or composites. The FEM codes were used to solve the Laplace equation: $(\nabla \cdot (\varepsilon \nabla V) = 0$, where ε is the relative permittivity and V is the local potential under

the border condition of plan-parallel capacitance. A procedure to generate random 3D microstructures similar to those provided by experimental SEM micrographs for the $BaTiO_3$ -polymer composites was developed , in which two types of filler geometries were compared: cubic (Figure 20) and spherical (Figure 21), respectively.

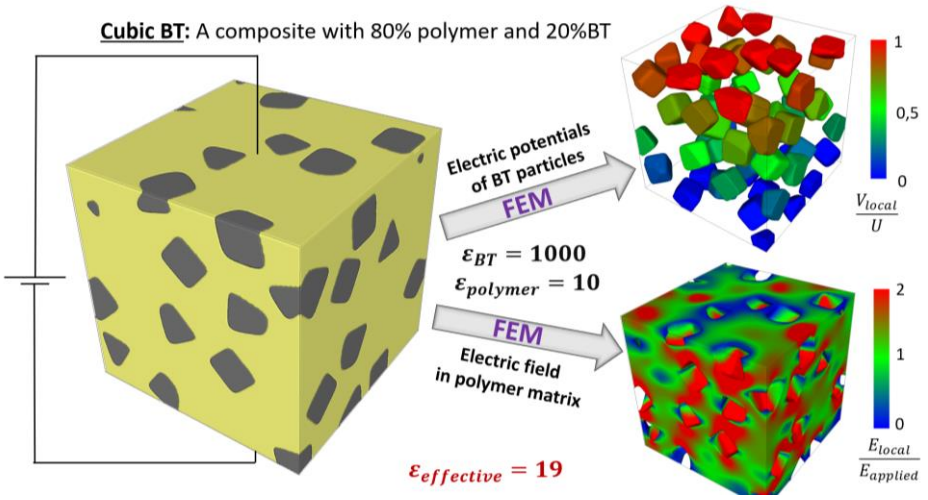

Figure 20. Simulation of local potential and fields and estimation of effective permittivity for a composite with 20% cubic $BaTiO_3$ nanoparticles within a polymer matrix.

The random cubic fillers were generated by the following procedure:

- Randomly generating of cube centers with coordinates: x_{ci}, y_{ci} și y_{ci}, where *i* is the cube index;
- Randomly generation of axes orientations by verctors $\overrightarrow{u_{xi}}$, $\overrightarrow{u_{yi}}$ și $\overrightarrow{u_{zi}}$;
- Building the cubes according to the equation: $\left(\frac{x^*}{10nm}\right)^6 + \left(\frac{y^*}{10nm}\right)^6 + \left(\frac{z^*}{10nm}\right)^6 = 1$, where x^*, y^* and z^* are the coordinates on the cube surface in the local coordinate system defined by the resors generated at the previous step.

The random spheroidalfillers were generated by the following procedure:

- Randomly generating of sphere centers with coordinates: x_{ci}, y_{ci} și y_{ci}, where *i* is the sphere index;
- Building the spheres according to the eq.: $\left(\frac{x-x_{ci}}{10nm}\right)^2 + \left(\frac{y-y_{ci}}{10nm}\right)^2 + \left(\frac{z-z_{ci}}{10nm}\right)^2 = 1$, where *x* , *y* and *z* are the coordinates of points on the i^{th} sphere surfaces in the capacitor coordinate system (i.e. Oz is the field direction, perpendicular on the electrodedsurfaces).

Simulations have shown that the *field distribution inside the composite is highly inhomogeneous* in both phases (polymer matrix and ferroelectric particles).

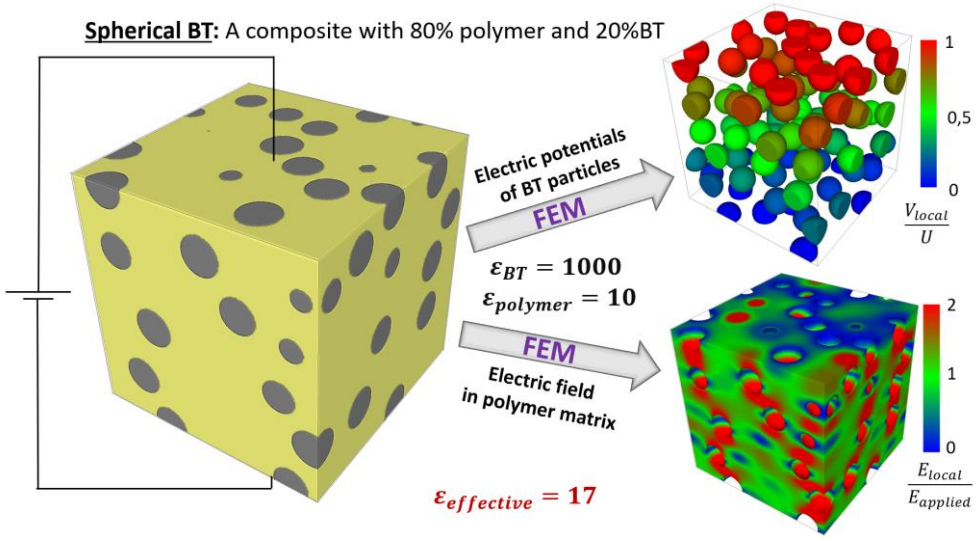

Figure 21. Simulation of local potential and fields and estimation of effective permittivity for a composite with 20% spherical $BaTiO_3$ nanoparticles within a polymer matrix.

For the same $BaTiO_3$ filler concentrations into the polymeric host matrix, it seems that there is a modest advantage of using cubic particles to increase the permittivity of the composite: for a polymer permittivity of $\varepsilon \approx 10$ and $\varepsilon \approx 1000$ for $BaTiO_3$ inclusions, in the composite with 20 wt.% filler, an effective permittivity of $\varepsilon \approx 19$ (nanocube inclusions) *vs.* $\varepsilon \approx 19$ ~17 (nanosphere inclusions) value was predicted. Although these values are relatively small for this combination of permittivity values, the increase is related to the property of field concentration at the corners and edges of the cube fillers.

In the next step, FEM simulations were aimed to determine the role of: (a) the filler concentration; (b) the particle size and (c) the particle size distribution on the effective permittivity and compare the results with those reported in the literature for similar systems and results reported by using effective field models, as well as to estimate the permittivity enhancement produced by a synergic effect of BTO and metallic nanoparticle fillers.

Thin layers made of close-packed $BaTiO_3$ nanocubes have been fabricated by depositing colloidal solutions containing 15 nm $BaTiO_3$ nanocubes, dispersed in toluene on both rigid (silicon, glass) and flexible substrates (flexible polyamide (Kapton), gelatin, etc.) followed by the controlled evaporation of the solvent. The surface size of the thin layer represented in Figure 22 is 20 by 20 microns, and the thin layer has a thickness of 300 nm.

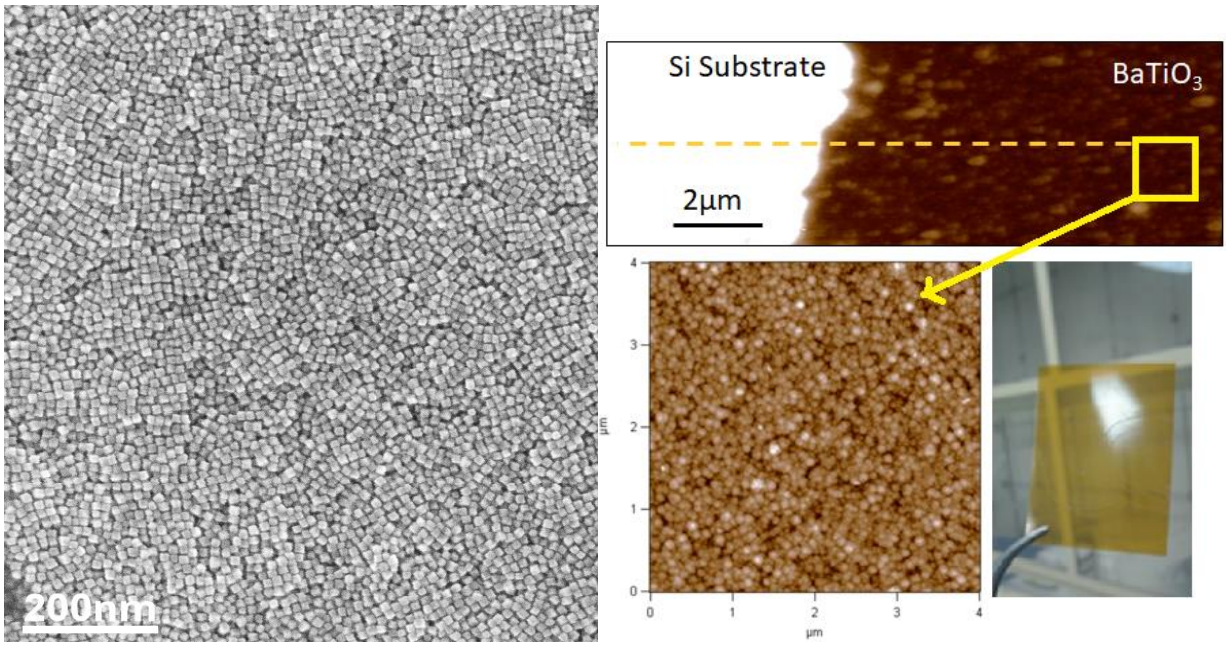

Figure 22. Scanning electron microscopy and AFM images of thin layers deposited on flexible polyimide substrate by direct deposition of colloidal nanoparticle solutions in toluene.

The thickness of the thin layers can be varied in a wide range of values, from tens of nanometers to tens of micrometers by varying both the concentration of nanoparticles in solution, the rate of evaporation of the solvent and the number of deposits made. As can be seen from Figure 22, the thin layers deposited on Kapton foils are transparent, which makes them very attractive for their use in the fabrication of flexible electronic components (planar capacitors or field effect transistors). Figure 23 shows representative scanning electron microscopy (SEM) images of $BaTiO_3$ thin films obtained by deposition from colloidal solutions. The resulting films consist of closely packed nanoparticles and their thickness was varied between 80 nm and 758 nm upon increasing the number of drops of solution cast on the substrate, either rigid or flexible. As a result, the number of deposited layers has increased from 1 to 7. As seen in the plot shown in Figure 23, upon optimizing the concentration of the nanocrystal inks, the thickness a thin layer obtained by casting one individual drop of solution on the substrate was about 100 nm. The thickness of the films and their roughness was routinely investigated by using atomic force microscopy (AFM).

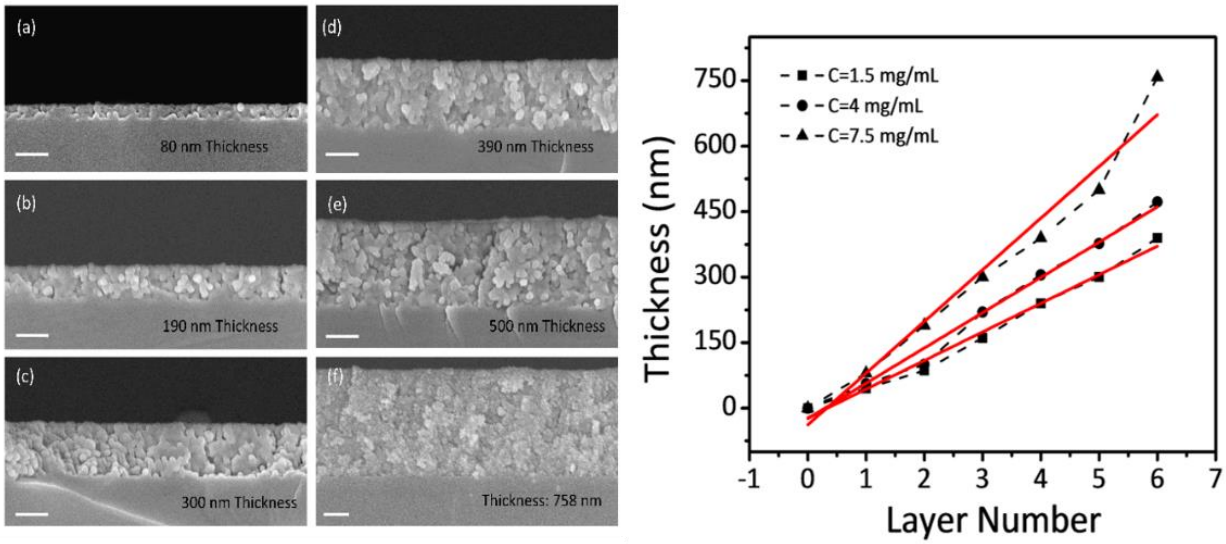

Figure 23. Scanning electron microscopy images of the cross-section of thin layers deposited on flexible polyimide substrate by direct deposition of colloidal solutions of nanoparticles in toluene. The graph on the right illustrates the variation of the thickness of thin layers containing $BaTiO_3$ nanocubes with a size of 15 nm as a function of the number of deposited layers.

In parallel with fabricating nanoparticle-based films by casting colloidal solutions of $BaTiO_3$ nanoparticles, the UAIC team used similar nanopowders compacted into pellets to investigate their properties by using different experimental techniques. *The goal of such experiments was two-fold*: *(1) to provide a reference basis for the optimization of the properties of thin films properties fabricated by using the same type of powders and (2) understand the interplay between the volume and surface/interface contributions to the functional properties of these dielectric materials. The related activities were extended during the first two years.*

To this end, bulk structures (thick films or ceramics) were prepared and investigated (Tasks 1 and 2; Stage 1)) being used as reference systems for the thin films produced from the same type of solutions of colloidal nanoparticles to understand the interplay between the volume and surface/interface contributions to their functional properties. In the frame of activities 1.1.3 and 2.1.3, ***a few types of bulk structures based on $BaTiO_3$ nanoparticles produced by the USV and UAIC teams were densified by the UAIC*** team using traditional and spark plasma sintering methods. Their dielectric, ferroelectric, tenability and the dielectric relaxation were determined. Since ferroelectric $BaTiO_3$ powders are excellent candidates for the design of magnetoelectric composite materials when interfaced with magnetostrictive phases, such as spinel ferrite oxides MFe_2O_4 (M= first series transition metal) the UAIC team performed some preliminary studies. Therefore, the UAIC team integrated ferroelectric $BaTiO_3$ thin films along with semiconductor ferrites in magnetoelectric multilayers and performed a comparative study of their properties in contrast with those of randomly mixed phases. Also, preliminary studies aimed at exploring the performance of porous $BaTiO_3$ nanostructures in gas sensing applications was tested, since the porosity of these dielectric layers makes them good candidates for gas sensing applications. Three main types of thick $BaTiO_3$-structures were studied.

III. 7. GHz – THz dielectric properties of flexible matrix embedded BTO nanoparticles

The dielectric properties of $BaTiO_3$ (BTO) nanoparticles and BTO-polymer composites described above were tested at high electromagnetic frequencies (30 GHz – 2 THz) using Time Domain Spectroscopy. Dielectric performances of the different materials obtained with different filler (nanoparticle) concentrations up to 40 wt. % embedded in gelatin, epoxy and styrene butadiene styrene (SBS) were compared at different working temperatures between 0 ^oC and 120 ^oC. Beside the general trend of ε' with the temperature, we were able to identify few matrix dependent optimal nanoparticle concentrations. The best composite performances were achieved by the BTO-SBS matrix, with filler concentration of 2% wt.,

where the losses have been of 1.5%, followed by BTO-gelatin matrix, with filler concentration of 40% wt, but with higher losses percent of almost 10% for THz frequencies.
Thus, three flexible materials were chosen for embedding BTO nanoparticles: gelatin, epoxy resin and styrene-butadiene (SBS) polymers. Below a brief description of each step will be presented.
Characterization Methods. Power absorption coefficients and refractive index for $BaTiO_3$ pellet (NP size 10 nm) have been measured in the spectral range 0.03 – 2 THz, with an average of 1800 scans and spectral resolution of $1cm^{-1}$ using the attenuated total reflectance module of a TPS3000 spectrometer from TeraView. The dielectric properties (real and imaginary parts), the phase shift and material loss factor (tan δ) of each material have been determined using the transmittance mode of the same equipment and with the same setting parameters. Each sample was placed in a mechanical holder having temperature control (0-120 ^oC), centered by the THz beam. Temperature dependence of the dielectric properties have been also investigated for each sample. Fig. 24a. shows the frequency dependence of the absorption coefficient which increases with the frequency up to 78 cm^{-1} corresponding to higher frequencies and with no prominent absorption peaks. This trend is similar with other literature results [Phys. Lett. A 372, (2008), pp. 2137-2140]; however, the absorption coefficient values are higher for our sample, at 1THz. Global absorption features did not significantly change by the temperature variation in the investigated range.

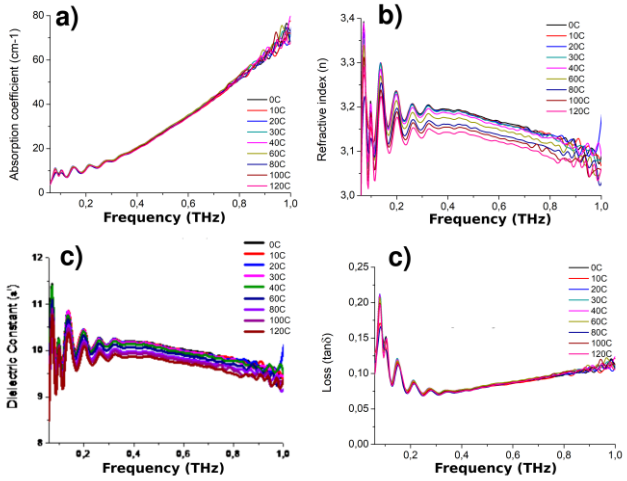

Figure 24. $BaTiO_3$ nanoparticle frequency dependent a) absorbance, b) refractive index, c) dielectric constant ε' and d) losses recorded in the temperature range from 0 ^oC to 120 ^oC.

However, the refractive index values decreased around 20% with the increasing the temperature , while a 40% decrease with the frequency could be estimated for the investigated range (Fig. 24b). The dielectric constant (ε') decreased by about 10% with the frequency within the investigated frequency range being affected by the temperature increase with less than 10% variation in the temperature range from 0 ^oC to 120 ^oC (Fig. 24c). The allure of the general loss curve suggests an optimal working frequency around 350 GHz and a 25% increase toward higher frequencies up to 1 THz and toward lower frequencies down to about 100 GHz. In other words, a three times higher or lower frequency will produce a similar increase of losses. It is worth noting that within the optimal frequency range, the temperature increase does not seem to substantially affect the values of the dielectric permittivity, whereas frequencies outside this range, and, in particular at lower frequencies losses (below 100 GHz) seem to be a lot more affected with percentages up to 25%.
In Table 1 are summarized the values of dielectric constant (real and imaginary components) for all studied samples for the frequency range from 60 Hz to 1 THz: pure $BaTiO_3$, pure SBS membrane, pure gelatin membrane, $BaTiO_3$ – gelatin nanocomposite with different weight percent of $BaTiO_3$ filler (6.25%, 18%, 25% and 40% wt.) and $BaTiO_3$ – epoxy with different weight percent of $BaTiO_3$ filler (2.8%, 5.4% and 10% wt.) and $BaTiO_3$ – SBS nanocomposite with different weight percent for $BaTiO_3$ filler (2%, 5% and 10% wt.) Evaluating the storage capabilities for all samples, we found that gelatin has the highest dielectric values (3.43) but with the largest losses percent (10%), followed by epoxy with 2.8 and losses of around 5 % from total storage. The best composite performances were achieved by the $BaTiO_3$-SBS matrix, with filler weight of 2%, where the losses have been of 1.5%, followed by $BaTiO_3$-gelatin matrix, with filler weight of 40%, but with higher losses percent, of almost 10%. To find out the origin of losses and energy storage in each matrix, we analyzed and presented in section below the phase change and dielectric properties changes in different temperature conditions for each type of material individually. Obtained composite dielectric performances in comparison with the pure nanoparticles and pure matrix performances we attributed to the NP-matrix interface contributions, both in the sense of dielectric performances and contribution in $BaTiO_3$ phase-change transition (temperature) points.

Table 1.

Sample	ε’	ε’’
BTO pellet 900 μm thickness		
100%	9 - 11.5 (0.06-1 THz), 9.45 (1THz)	0.5 - 2 (0.06-1 THz), 0.99 (1THz)
BTO – SBS		
0%	1 – 2.5 (0.06 -2 THz), 2.1 (1THz)	0.001 – 0.6 (0.06 -2 THz), 0.007 (2THz)
2% 10nm	1.7 - 5.3 (0.06 -2 THz), 4.1 - 4.5 (2 THz)	0.1 – 1.6 (0.06 -2 THz), 0.07 (2 THz)
2% 20 nm	0.8 – 2.7 (0.06 -2 THz), 2 (2 THz)	0.4 - 0.5 (0.06 -2 THz), 0.025 (2 THz)
5% 10 nm	0.3 – 7 (0.06 -0.1 THz), 1.96 (2 THz)	0.3 - 5.5 (0.06 -0.1 THz), 0.3 (0.1-2 THz)
5% 20 nm	0.2 – 6.5 (0.06 -0.1 THz), 1.95 (2 THz)	0.1 – 2.4 (0.06 – 2 THz), 0.016 (2 THz)
10% 10 nm	0.6 - 2.4 (0.06 – 2 THz) 1.44 (2 THz)	0 – 0.7 (0.06 – 2 THz) 0.007 (2 THz)
10% 20 nm	3.8 – 0.04 (0.06 – 2 THz) 1.35 (2 THz)	0.05 - 2 (0.06 – 2 THz) 0.002 (2 THz)
BTO – Gelatin		
0%	2.2– 5.7 (0.06 -2 THz), 3.43 (2 THz)	0.1 – 1.5 (0.06 -2 THz), 0.37 (2 THz)
6.25%	3.5 - 4.5 (0.06 -2 THz), 3.66 (2 THz)	0.2 – 1.6 (0.06 -2 THz), 0.34 (2 THz)
18%	3.5 – 5 (0.06 -2 THz), 3.55 (2 THz)	0.2 – 1 (0.06 -2 THz), 0.37 (2 THz)
25%	3.6 – 5.3 (0.06 -2 THz), 3.9 (2 THz)	0.3 – 1.3 (0.06 -2 THz), 0.44 (2 THz)
40%	3.9 – 6.6 (0.06 -2 THz), 4.11 (2 THz)	0.4 – 2.4 (0.06 -2 THz), 0.53 (2THz)
BTO- epoxy		
0%	2.6 - 2.8 (0.06 – 2 THz)[14}	0 - 0.15 (0.06 – 2 THz)[14}
2.8%	2.6 – 3.5 (0.06 – 2 THz), 3.16 (2 THz)	0.1 – 0.4 (0.06 – 2 THz), 0.13 (2 THz)
5.4%	2.9 – 4.2 (0.06 – 2 THz), 3.2 (2 THz)	0.09 – 1.4 (0.06 – 2 THz), 0.13 (2 THz)
10%	3 – 3.7 (0.06 – 2 THz), 3.19 (2 THz)	0.08 – 0.7 (0.06 – 2 THz), 0.16 (2 THz)

III. 8. Design of Rigid and Flexible Capacitors by Using $BaTiO_3$ Nanoparticles as Building Blocks

Both sets of $BaTiO_3$ nanoparticles with cubic and dodecahedron morphology have been integrated into rigid and flexible capacitors. For the fabrication of the rigid capacitors, the dielectric thin films have been deposited on silicon and glass substrates. Au and Ag have been used as electrodes with a circular shape of 1.5 mm in diameter. Figure 25 shows the rigid capacitors that integrates cubic shape $BaTiO_3$ nanoparticles and it’s performance and Figure 26 shows the rigid capacitors that integrates dodecahedron shape nanoparticles.

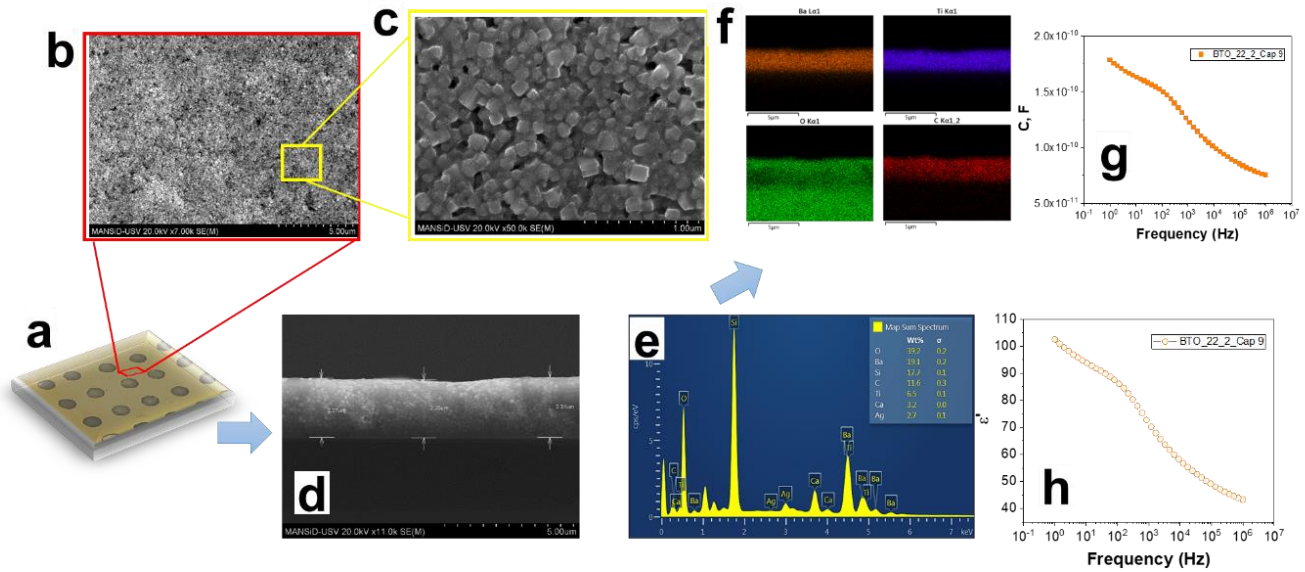

Figure 25. Fabrication of capacitors on a rigid substrate, which include thin film of BaTiO3 with cubic morphology. The thin films were obtained from colloidal solutions, by drop casting (a-d). Elemental analysis of thin layers (e-f) and electrical characterization of capacitors (g-h) respectively.

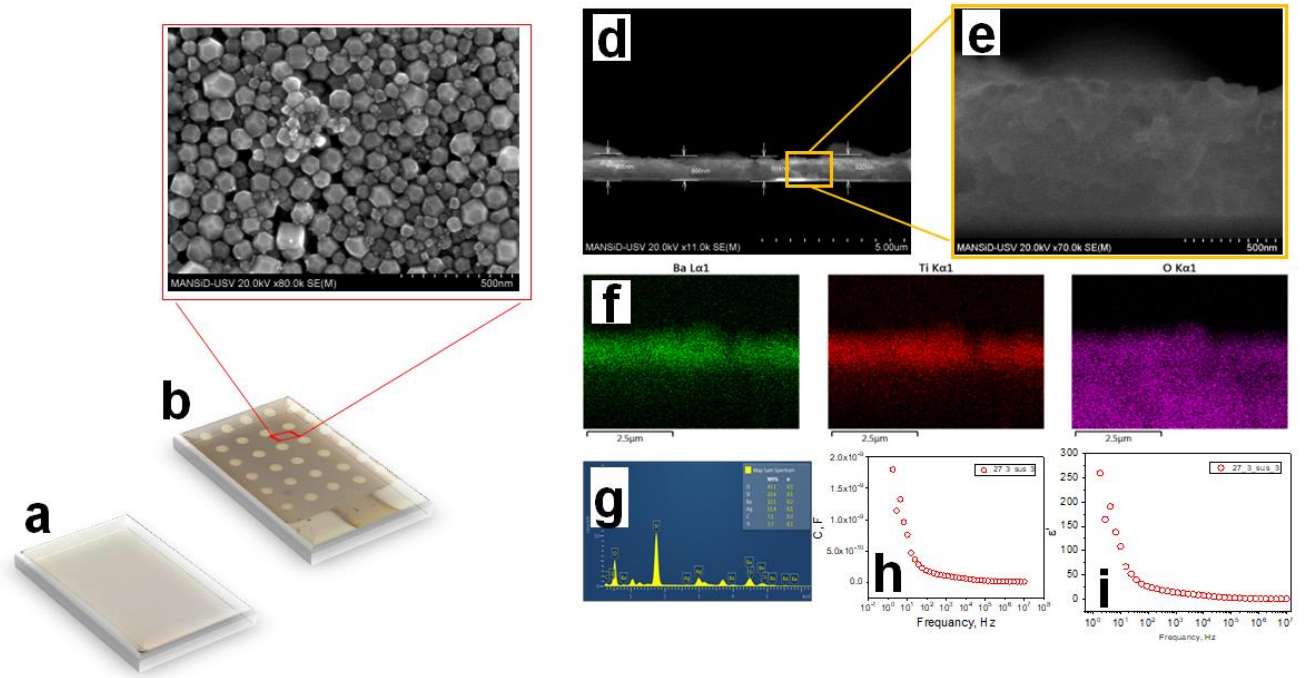

Figure 26. Fabrication of capacitors on rigid substrate, which include thin film of $BaTiO_3$ with dodecahedral morphology. The thin films were obtained from colloidal solutions, by drop casting (a-e). Elemental analysis of thin films (e-g) and electrical characterization of capacitors (h-i) respectively.

A schematic representation of the geometry of flexible capacitors along with an image of a cross section of a thin layer of $BaTiO_3$ nanocubes are provided in Figure 27a. Figure 27b shows the graphs corresponding to the leakage currents on the surface unit of the dielectric thin layer, as well as the curve describing the dependence of the leakage current as a function of the applied voltage (J_{leak}-V). Preliminary data indicated the presence of a leakage current in the dielectric layers after the application of a voltage of 4 V (corresponding to a current density of ($\sim 8 \times 10^{-5}$ A/cm^2), which suggests that these thin layers can operate in the range of voltage between 0 and 4 V.

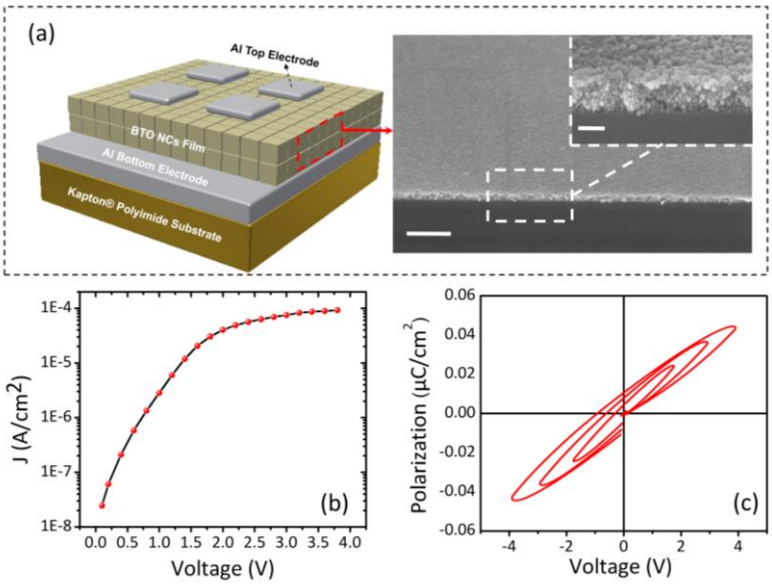

Figure 27. Diagram of a planar capacitor made of thin layers containing $BaTiO_3$ nanocubes with a size of 15 nm and the dielectric characteristics of this capacitor.

The dielectric polarization of this capacitor was measured according to the voltage applied at a frequency of 100 Hz. From the curve describing the behavior of the thin layer can be seen the presence of a nonlinear behavior, suggesting that the thin layer has ferroelectric properties, with a residual polarization P_s of approximately 0.011 $\mu C/cm^2$ at a maximum voltage of 4 V.

III. 8. Design of flexible field effect transistors by using $BaTiO_3$ nanoparticles as building blocks

Proof-concept experiments were aimed at incorporating dielectric nanocrystal-based $BaTiO_3$ thin films were incorporated into transparent and flexible field effect transistors (FETs) whereby the semiconducting channel was fabricated from a 10 nm In_2O_3 nanoparticle-based film. FETs exhibited high-performance n-type characteristics with a small hysteresis (0.1 ± 0.04 V) and a subthreshold swing SS = 808 mV $decade^{-1}$ at an operating voltage of 10 V. This study provides a simple, yet highly versatile low-cost alternative for the fabrication of flexible electronic devices such as capacitors and FETs with superior performance characteristics by using colloidal inks containing both high capacitance gate dielectric and semiconducting colloidal nanocrystals. Nanoparticle inks were fabricated by suspending the oleic acid passivated $BaTiO_3$ and In_2O_3 colloidal nanocrystals in a nonpolar solvent, such as toluene, followed by sonication. No other stabilizers were used since, as we showed previously, the oleic acid molecules passivating the surface of the colloidal nanocrystals will enable them to be dispersible in nonpolar solvents.

Below are presented relevant data pertaining to the design of FETs by using close-packed nanoparticulate BTO films deposited on 50 μm polyimide flexible substrates (Kapton). The films were deposited from dielectric inks obtained by dispersing 15 nm $BaTiO_3$ nanocubes in toluene followed by drop casting and the slow evaporation of the solvent under ambient conditions. The semiconducting layer had an average thickness of 60 nm and consisted of a thin film made of spherical In_2O_3 colloidal nanocrystals obtained by a solution-based method, whereas the thickness of the dielectric film was about 100 nm. The FET was designed by depositing source and drain 50 nm Al electrodes by a thermal evaporation process upon a lift-off process. Figure 27 shows a picture of the dielectric ink containing 15 nm $BaTiO_3$ nanocubes (shown in the next picture as a top-down TEM image), a schematic of the FET and the image of the FET with a channel length ratio W/L of 10).

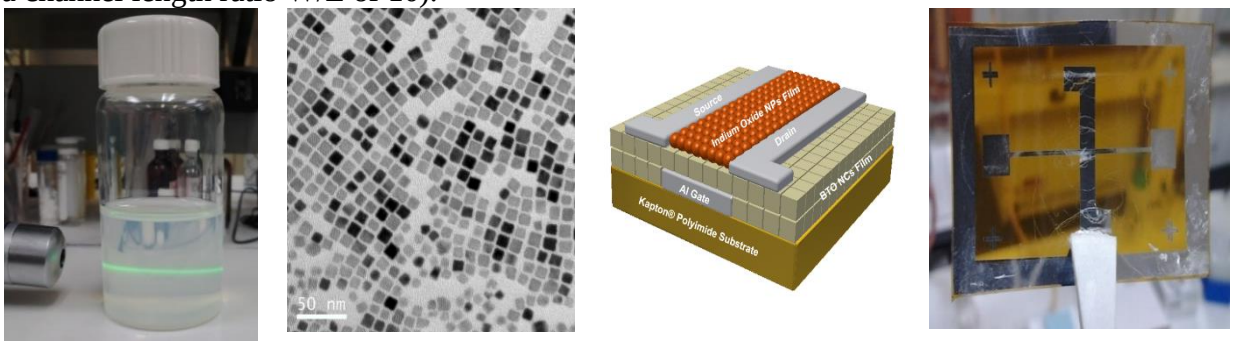

Figure 27. Dielectric ink containing 15 nm $BaTiO_3$ nanocubes (shown in the next picture as a top-down TEM image), a schematic of the FET and the image of the FET with a channel length ratio W/L of 10).

Figure 28b shows the transfer characteristics for the $BaTiO_3/In_2O_3$ thin film transistor. As can be easily inferred, the transistor is characterized by a threshold voltage of 2.9 ± 0.05 V and possesses a very small hysteresis (0.1 ± 0.04 V). Moreover, the extracted values of the on/off ratio and subthreshold swing are Ion/Ioff B 104 and SS = 808 mV decade^{-1}. The subthreshold swing (SS) is the inverse of the subthreshold slope of the log drain current vs. the gate voltage (VG) below the threshold voltage (Vth), which defines the boundary between the subthreshold and transport regimes. Similarly, the carrier mobility was determined from the slope of the drain–source current (IDS) vs. the gate voltage (VG), as described by the equation:

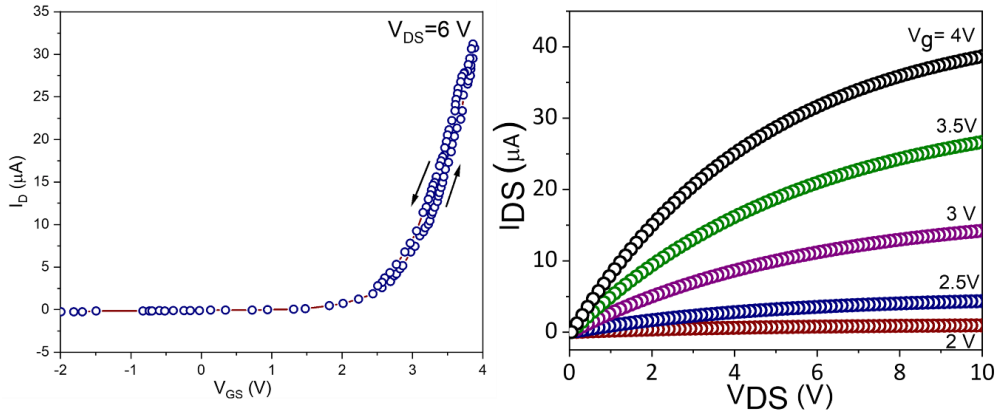

(a) **(b)**

Figure 28. Electrical performance of the BaTiO3/In2O3 flexible transistor: typical output (b) and transfer (c) characteristics of the flexible, transparent FET.

The calculated carrier mobility was μ_{eff} = 17.4 ± 0.2 cm^2 V^{-1} s^{-1}, a value which is higher than that reported in the literature for both inorganic and organic field effect transistors containing $BaTiO_3$ nanoparticle films as the gate dielectric, which suggests that the $BaTiO_3$ colloidal nanocrystals obtained by this synthetic method exhibit great potential for integration into flexible field-effect transistors with superior performance characteristics. The experimental data confirmed the excellent n-type characteristics of the FET at low operating driving voltages. This is presumably facilitated by a low trapped state density, which will require the injection of a lower concentration of charge carriers. In turn, the trapped states at the dielectric/semiconductor interfaces are ascribed to the existence of surface defects, which can influence the charge transport by scattering and/or trapping the charges at the interfaces. This clearly demonstrates that the rigorous selection of inorganic colloidal nanocrystals with controlled morphology and surface composition and their assembly into thin film structures via solution processing is a viable method for the design of flexible FETs with superior performance characteristics. Combining the optimized dielectric gate with an In_2O_3 quantum dot semiconductor channel affords significant generality in the fabrication of solution-processed thin film transistors with I_{on}/I_{off} ~ 10^4 operating at voltages as low as ~10 V.

III. 9. Integration of Oxide Layers (semiconductor and dielectric) in Flexible Inverters- and Characterization of their DC Conversion Characteristics. Preliminary tests were performed on TFTs, to investigate their ability to function as switches for inverters. To this end,, a rectangular signal generator was used to apply a voltage to the gate, closing and to open the conduction channel. The output signal from the source was collected from a load resistor. The variations of the voltage of the resistor were recorded with a digital oscilloscope and are presented in Figure 29 for two types of functional transistors.

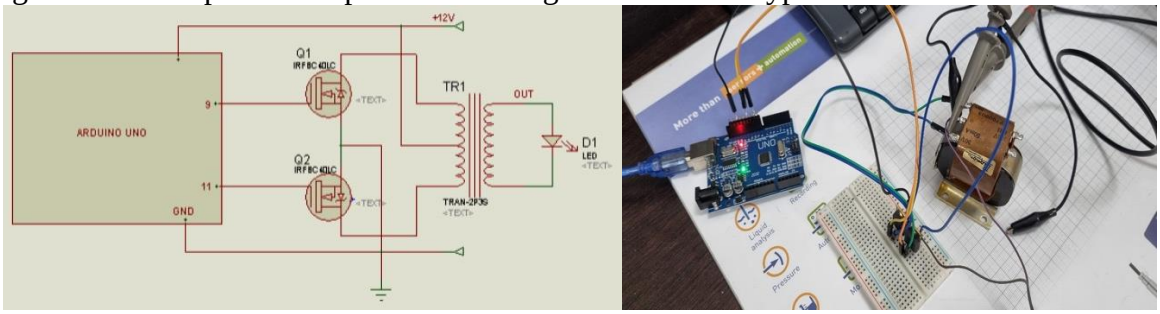

Figure 29. From left to right and from top to bottom: inverter diagram; experimental assembly; transistor drain signal and inverter output signal, respectively.

However, the drain currents are too small for a decent operation, requiring an amplification before being used in the actual inverter part.

IV. Dissemination in terms of remarkable publications

The results obtained during the implementation of HIGHkDEVICE project have been disseminated in 24 published ISI articles, 3 articles which are presently under review and 34 presentations at national and international conferences. Furthermore, another 3 articles are under preparation and will be submitted soon, as well as a patent on the synthesis process of BaTiO3 nanocubes with dimensions larger than 100 nm. More details on the dissemination of the results from this project can be found on the project‘swebsite at : http://nanomat.usv.ro/pagina-05-5-c.php.

PhD Thesis defended, (team members are underlined):

1. Vlad Alexandru Lukacs, “*Scale dependent effects in ferroelectric oxides*”, “Al.I. Cuza” University, Iasi, 2020.
2. Ina Turcan, “*Ceramic composites with multifunctional properties*”, “Al.I. Cuza” University, Iasi, 2021.

Ph.D thesis which will be defended in the first part of 2023 (team members are underlined):

1. Vasyl Michaylovich, *“Nanoscale Ferroic Materials for the Rational Design of Electronic Devices”,* Stefan cel Mare University, Suceava. The thesis defense is scheduled for April 2023.
2. Maria-Iuliana BOGDAN (căs. CHIRICĂ), “*Layered 2D and 3D nanostructures for applications in flexible electronics and catalysis”,* Institutul National de Cercetare – Dezvoltare pentru Fizica Materialelor Bucuresti RA. The thesis defense is scheduled for the beginning of 2023

Master thesis defended (team members are underlined)**:**

[1] Radu-Stefan Stirbu, Mesoscale models for strain-stress fields in porous ceramics, “Al.I. Cuza” University, Iasi, June 2022

[2] Teodora Matei, $BaTiO_3$-based ferroelectric ceramics for energy storage and harvesting, “Al.I. Cuza” University, Iasi, June 2022

Estimated impact of the HIGHkDEVICE project, and the most prominent result

This project contributed significantly to the development of a robust predictive methodology for the assembly of of ferroelectric nanoparticles into dense, defect free high-k dielectric layers and their subsequent incorporation into functional devices, such as capacitors and field effect transistors on both rigid and flexible substrates by using simple, highly feasible, yet inexpensive solution processing techniques. The design of “all inorganic” flexible field effect transistors can constitute an important way to make inroads to inexpensive, high quality functional electronic devices for modern circuitry.

Project Director
conf. univ. dr. Aurelian Rotaru